NOAA Project
Report

Tsunami Inundation Maps Development for the Gulf of Mexico

Final Report to the
National Tsunami Hazard Mitigation Program (NTHMP)
in Completion of Project Awards
NA23NWS4670020

Authors

Juan J Horrillo Texas A&M University at Galveston
Wei Cheng

Collaborators:

Under the guidance of
NTHMP Mapping and Modeling Subcommittee

National Tsunami Hazard Mitigation Program

National Oceanic and Atmospheric Administration

Ocean Engineering
Texas A&M University at Galveston
Galveston, Texas, 77553

December 2024

Contents

List of Figures

List of Tables

1 Executive Summary

Potential tsunami sources for the GOM are local submarine landslides, which have been examined in the past by the Atlantic and Gulf of Mexico Tsunami Hazard Assessment Group [ten Brink et al., 2009b]. In their findings, they stated that submarine landslides in the GOM are considered a potential tsunami hazard. However, the probability of such an event (tsunamis generated by large landslides) is low. The probability of occurrence is related to ancient (geological) massive landslides which were probably active prior to 7,000 years ago when large quantities of sediments were emptied into the Gulf of Mexico. Nowadays, sediment continues to empty into the Gulf of Mexico mainly from the Mississippi River. This sediment supply contributes to the slope steepening and the increase of fluid pore pressure in sediments, which may lead to further landslide activities and hence, the reason for this study in determining the potential tsunami hazard and its effects in the Gulf of Mexico.

For the triggering mechanism (tsunami generation) we use five geological sources, i.e., the Eastbreaks, Mississippi Canyon, West Florida landslides, and two Yucatán landslides introduced in [Horrillo et al., 2018]. A probabilistic approach was implemented in our previous study, see [Horrillo et al., 2015], to fill gaps along the continental shelf between the geological landslide sources by adding synthetic landslide sources (four in total) to cover the entire northern part of the GOM. Our probabilistic approach confirmed a recurrence period of major landslide events of around 8000 years, consistent with findings by [Geist et al., 2013].

These geological and probabilistic tsunami sources (nine in total) are used as the maximum credible events that could happen in the region according to the local bathymetry, seafloor slope, and sediment information. These credible events are then used to determine the inundation impact on selected communities along the GOM. The extent and magnitude of the tsunami inundation in those selected locations are achieved by using a combination of 3D and 2D coupled-numerical models. For instance, the 3D model, TSUNAMI3D, is used for tsunami generation to determine the initial dynamic wave or initial source and results are passed as an input to the 2D non-hydrostatic model, NEOWAVE, to determine the tsunami wave propagation and the detailed runup and inundation extent in each of the communities. Tsunami flooding inland-extent, maximum inundation water depth, momentum flux and direction, current velocity and vorticity can then be determined within the inundation-prone areas of the selected communities. Also, tsunami inundation and hurricane category flooding can be compared to access tsunami hazard in unmapped locations.

This project focused on the implementation of recent developments in the tsunami science recommended by the National Tsunami Hazard Mitigation Program - Modeling Mapping Subcommittee - Strategic Plan (NTHMP-MMS-SP) into our current Gulf of Mexico (GOM) tsunami mitigation products. Four main developments for tsunami mitigation have been created under this project for communities in the GOM that will provide guidance to state emergency managers for tsunami hazard mitigation and warning purposes.

The first is the development of tsunami inundation maps in Rosemary Beach, FL and North Tampa Bay, FL. Maximum tsunami inundation extent, water height, and momentum flux magnitude and direction are determined from each landslide sources, as well as the maximum of maximum inundation maps from all nine landslide sources. The two new

tsunami inundation map products add to the existing 20 mapped locations, which provide so far good coverage of the most populous coastal areas along the GOM.

The second is a continuing study of the comparison between existing SLOSH hurricane flooding data and our tsunami inundation result, in order to provide temporal-low-order estimate for tsunami hazard areas (community) where inundation studies have not yet been assigned/executed or where little bathymetric and elevation data exists. The adopted approach to define a quick estimate of tsunami vulnerability areas in the GOM has been taken from the existing hurricane storm surge flooding results along coastal areas, in which storm flooding map products are based on hurricane category. The existing storm surge flooding maps cover almost the entire GOM coastal regions and thus they are very well known among GOM regional emergency managers and other parties.

The third is to produce the velocity and vorticity magnitude maps for all the landslide scenarios, for Rosemary Beach, FL and North Tampa Bay, FL. Based on these maritime maps, location of strong currents and their damaging levels are identified. The tsunami hazard maritime products such as tsunami current magnitude, vorticity, safe/hazard zones would be central for future developments of maritime hazard maps, maritime emergency response and as well as infrastructure planning. We hope that the results herein may assist the maritime communities, port managers and other NTHMP's interested parties.

?????The fourth task is a continuation of the study to obtain an understanding of meteotsunami through the characterization of physical parameters in GOM [Cheng et al., 2021, Horrillo et al., 2020, 2021]. In this project, we expanded the previous parameter study from 1260 runs (on 1 arcminute resolution grid) to 17280 runs (15 arcsecond grid) for each subregion (northeastern & northwestern GOM), thanks to the huge performance increase using CUDA on our newly built multi-GPU workstation. The GPU workstation is able to run our meteotsunami CUDA Fortran code 50 – 100 times faster than it CPU versoin, depending on the grid. The result is a significantly improved resolution of different incident wave direction, forward speed and trajectory position, and their effect on maximum gauge water elevation across the whole GOM. In addition, characterization of meteotsunamis in northern GOM using meteotsunami rose charts and an application of ANN in meteotsunami water elevation prediction are performed on the new data generated from the parameter study

Although the recurrence of destructive tsunami events have been verified to be quite low in the GOM, our work has confirmed that submarine landslide events with similar characteristics to those used here, have indeed the potential to cause severe damage to GOM coastal communities. Therefore, this work is intended to provide guidance to local emergency managers to help managing urban growth, evacuation planning, and public education with final objective to mitigate potential tsunami hazards in the GOM.

2 Introduction

2.1 Background

The U.S. Tsunami Warning System has included Gulf of Mexico (GOM) coasts since 2005 in order to enable local emergency management to act in response to tsunami warnings. To

plan for the warning response, emergency managers must understand what specific areas within their jurisdictions are threatened by tsunamis. Coastal hazard areas susceptible to tsunami inundation can be determined by historical events, by modeling potential tsunami events (worst-case scenarios), or by using a probabilistic approach to determine the rate of recurrence or likelihood of exceeding a certain threshold. As the GOM coastal regions have no significant recent historical tsunami records, numerical modeling and probabilistic methodologies for source identification must be used to determine coastal hazard zones.

Potential tsunami sources for the GOM are local submarine landslides [ten Brink et al., 2009b]; sources outside the GOM are considered a very low threat and may not significantly impact GOM coastal communities or infrastructure [Knight, 2006]. Although a massive tsunamigenic underwater landslide in the GOM is considered a potential hazard, the frequency of such events (though not well-constrained) is probably quite low based on historical evidence [Dunbar and Weaver, 2008] and available data on ages of failures which suggest they were probably active prior to 7,000 years ago when large quantities of sediments were emptied into the GOM [ten Brink et al., 2009b]. However, sediments continue to empty into the GOM, mainly from the Mississippi River, contributing to slope steepening and the increase of fluid pore pressure in sediments which may lead to unstable slopes that can be subsequently triggered to failure by seismic loading [Masson et al., 2006, ten Brink et al., 2009a, Dugan and Stigall, 2010, Harbitz et al., 2014]. In addition, the unique geometry of the GOM basin makes even unlikely tsunami events potentially hazardous to the entire Gulf Coast. Waves tend to refract along continental slopes; thus, given the curved geomorphology of the GOM shelf and the concave shape of the coastline, any outgoing tsunami wave could potentially affect the opposite coast in addition to the coast close to the landslide source.

Five large-scale geological submarine landslides with tsunamigenic potential have been identified within the GOM [ten Brink et al., 2009b, Chaytor et al., 2016], representing possible worst-case tsunami scenarios affecting GOM coasts in the past. In order to generate a more complete picture of landslide tsunami potential in the GOM, a probabilistic approach has been implemented to develop four additional synthetic landslide sources which fill gaps along the continental shelf between the geological landslide sources [Pampell-Manis et al., 2016]. These probabilistic tsunami sources are considered to be the maximum credible events that could happen in a particular region of the GOM according to the local bathymetry, seafloor slope, sediment information, and seismic loading. The probabilistic maximum credible events together with the geological sources form a suite of tsunami sources that have been used within coupled 3D and 2D numerical models to model tsunami generation and propagation throughout the GOM and to develop high-resolution inundation maps for the inundation-prone areas of two new communities along the Gulf Coast: Rosemary Beach, FL and North Tampa Bay, FL. These inundation studies showed that tsunamis triggered by massive submarine landslides have the potential to cause widespread and significant inundation of coastal cities. All of the 23 communities from both previous and current work and nine landslide sources are shown in Fig. 1.

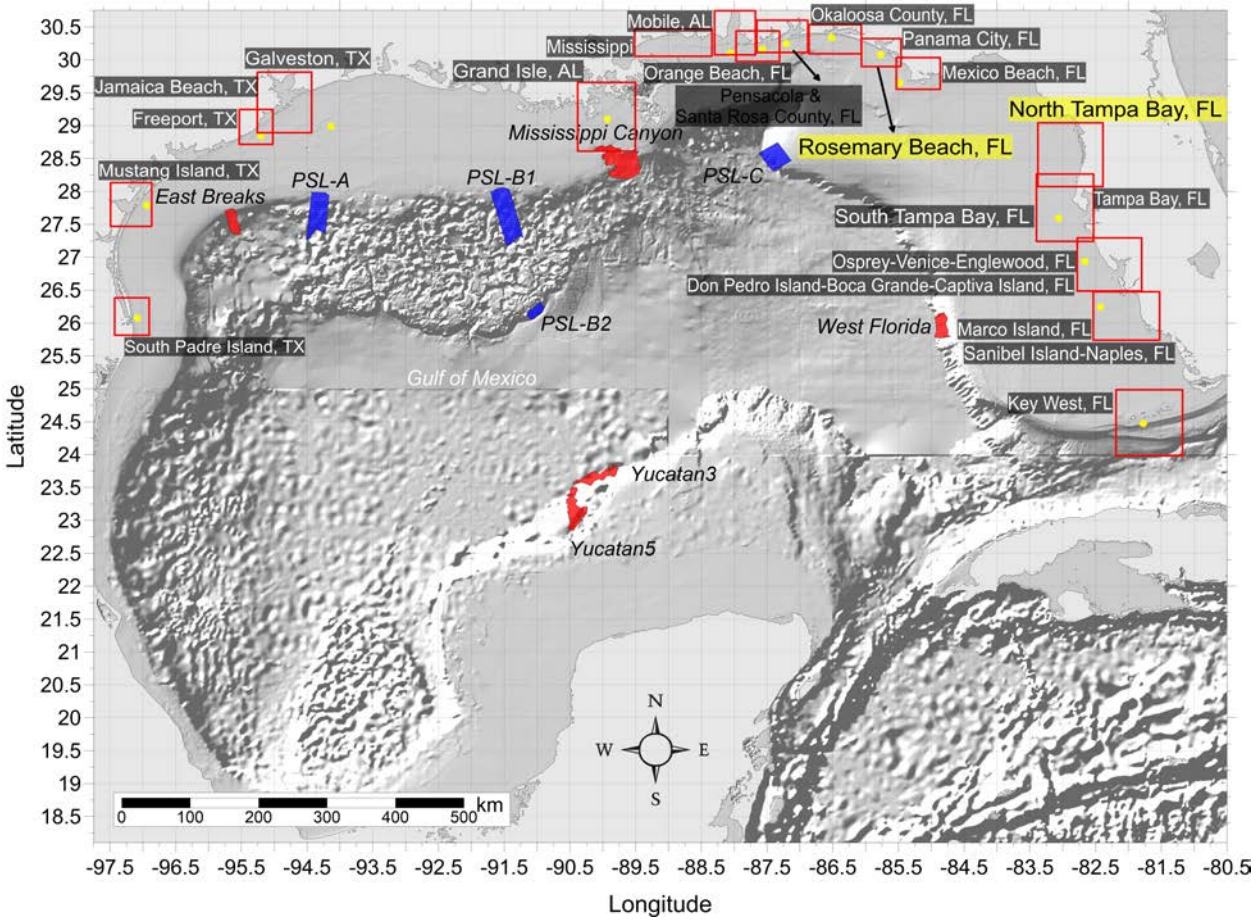

Figure 1: Selected communities or geography regions along the US GOM coastline where tsunami maps have been developed. Red rectangles denote 3 arcsecond (∼90m) domains of coastal communities where tsunami inundation has been modeled (highlighted Mississippi is developed in the current project); red hatched areas are geological landslide sources; blue hatched areas are Probabilistic Submarine Landslide (PSL) sources; yellow dots are locations of numerical wave gauges. The zero-meter elevation contour is drawn to show the GOM coastline.

While high-resolution tsunami inundation studies have been completed for these 23 communities and are planned for additional locations, vulnerability assessments are still essential for coastal locations where inundation studies have not yet been performed or planned, or where there is a lack of high-resolution bathymetric and/or elevation data. Therefore, we aim to extend the results of the completed mapping studies in order to provide estimates of tsunami inundation zones for hazard mitigation efforts in unmapped locations. Inundation maps with even low resolution are useful to emergency managers to create first-order evacuation maps, and some methods currently exist to provide low-resolution estimates of hazard zones for regions which do not currently have or warrant high-resolution maps. For example, guidance given by the National Tsunami Hazard Mitigation Program (NTHMP) Mapping and Modeling Subcommittee in "Guidelines and Best Practices to Establish Areas of Tsunami Inundation for Non-modeled or Low-hazard Regions" (available from `https://nws.weather.gov/nthmp/documents/3nonmodeledregionguidelines.pdf`) recommends that coastal areas and areas along ocean-connected waterways that are below 10 m (33 ft) elevation are at risk for most tsunamis, and rare and large tsunamis may inundate above this elevation. However, in low-lying coastal regions such as along the Gulf Coast, the 10 m (33 ft) elevation contour is too far inland to be reasonably applicable for estimating potential tsunami inundation zones. The guidance additionally suggests that low-lying areas are prone to inundation within 3 km (1.9 mi) inland for locally-generated tsunamis and within 2 km (1.3 mi) inland for distant sources. While these distances may be reasonable for some regions of the Gulf Coast, prevalent bathymetric and topographic features such as barrier islands/peninsulas complicate the method of delineating inundation-prone areas based on distance from the shoreline. As a result, the purpose of the current work is to improve the methodology which compares modeled tsunami inundation to modeled/predicted hurricane storm surge. Specifically, we aim to identify the hurricane category which produces modeled maximum storm surge that best approximates the maximum tsunami inundation in the two new locations modeled in this project. Even though many physical aspects of storm surge inundation are completely different from those of tsunamis (time scale, triggering mechanism, inundation process, etc.), good agreement or clear trends between tsunami and storm surge flooding on a regional scale can be used to provide first-order estimates of potential tsunami inundation in communities where detailed inundation maps have not yet been developed or are not possible due to unavailability of high-resolution bathymetry/elevation data. Additionally, since tsunamis are not well-understood as a threat along the Gulf Coast, while hurricane hazards are well-known, this method of predicting tsunami inundation from storm surge provides a way for GOM emergency managers to better prepare for potential tsunami events based on more understandable and accessible information. This hurricane-tsunami comparison was first carried out in Horrillo et al. [2016] (award number NA14NWS4670049) where five previously mapped locations were studied, namely South Padre Island, TX, Galveston, TX, Mobile, AL, Panama City, FL, and Tampa, FL; then as a regular procedure for all the newly mapped locations during the following mapping projects.

Past tsunamis have shown that the maritime community requires additional information and guidance about tsunami hazards and post-tsunami recovery [Wilson et al., 2012, 2013]. To accomplish mapping and modeling activities to meet NTHMP's planning/response purposes for the maritime community and port emergency management and other customer

requirements, it is necessary to continue the process to include maritime products in our current inundation map development. These activities will include tsunami hazard maritime products generated by GOM's tsunami sources (submarine landslides) that may impact specifically ship channels, bay inlets, harbors, marinas, and oil infrastructures (e.g., designated lightering and oil tanker waiting zones), which has already been applied in other tsunami risk regions, e.g., California, Oregon and Washington. It is worth noting that Galveston was the first city where we implemented the maritime products [Horrillo et al., 2016]. South Padre Island, TX, Mobile, AL, Panama City, FL, and Tampa, FL, Pensacola, FL, Key West, FL, Okaloosa County, FL, Santa Rosa County, FL and Mustang Island, TX, were implemented in project NA15NWS4670031 and NA16NWS4670039 [Horrillo et al., 2017], and then as a regular procedure for all the newly mapped locations during the following mapping projects.

2.2 Regional and Historical Context

This project covers the entire Mississippi coastlines.

All the locations and cities mentioned in the following regional context are in Mississippi, so the shortcut MS for the state will be omitted from here on.

The first 1/3 arcsecond resolution mapping area (grid 4) covers the western MS coastlines, including Waveland, Bay St. Louis, Pass Christian, Long Beach, and Gulfport. The second 1/3 arcsecond resolution mapping area (grid 5) covers Biloxi, D'Iberville, Ocean Springs, Gautier, and Pascagoula. The barrier islands protecting the coastal cities of Mississippi are part of the Gulf Islands National Seashore. These islands, running from west to east, are: Cat Island, Ship Island, Horn Island and Petit Bois Island. These islands act as natural barriers, shielding the Mississippi Gulf Coast from storm surges, waves, and hurricanes.

Mississippi's coastal cities are protected by several major bays and barrier islands. The key bays include Bay St. Louis, Biloxi Bay, Back Bay of Biloxi, St. Louis Bay, Pascagoula Bay, and Grand Bay, each playing a significant role in the region's coastal geography. These bays, while offering natural harbors and supporting local ecosystems, can also funnel storm surges inland, increasing the risk of flooding during hurricanes.

In the event of a hurricane, major evacuation routes are vital. Interstate 10 (I-10) serves as the primary east-west corridor across southern Mississippi, linking to Louisiana and Alabama, while U.S. Highway 90 (US 90) runs parallel to the coast for local evacuations. Interstate 59 (I-59) offers a route northeast through Hattiesburg, while Mississippi Highways 603, 49, and 67 provide crucial inland connections from the coastal areas. These roads form the backbone of Mississippi's hurricane evacuation plan, guiding residents safely away from the coast.

Coastal protection efforts in Mississippi have been ongoing, particularly following the devastating impacts of hurricanes like Katrina in 2005. These efforts include the construction of seawalls, the restoration of wetlands, and the reinforcement of levees to reduce flood risks. Additionally, barrier island restoration projects, such as the ongoing work on Ship Island, aim to maintain these critical natural barriers. These efforts are vital for protecting the coastal communities, as they mitigate the effects of hurricanes and preserve the region's natural defenses against future storms.

The coastal cities of Mississippi, stretching from west to east, have experienced varying population changes between the 2010 and 2020 U.S. Census. Waveland saw a decrease of 5.9%, with its population dropping from 6,435 to 6,056. In contrast, Bay St. Louis grew by 9.8%, reaching 10,170 residents in 2020. Pass Christian experienced significant growth, with a 20.6% increase, bringing its population to 5,564. Long Beach also saw a rise of 13.9%, reaching 16,855 people. Gulfport, the second-largest city on the coast, grew by 7.6%, reaching a population of 72,926. Biloxi, another major city, saw a 12.3% increase, with 49,449 residents by 2020. D'Iberville experienced the highest growth rate among these cities, with a 54.5% increase to 14,657. Ocean Springs had a modest increase of 4.8%, with 18,275 residents, while Gautier grew by 2.6%, reaching 19,055 people. Lastly, Pascagoula saw a slight decrease of 3.2%, with its population declining to 21,685. These population shifts reflect the dynamic changes occurring along Mississippi's Gulf Coast.

Mississippi's Gulf Coast has experienced several major hurricanes that have caused significant damage, particularly due to their storm surges and high winds. Notable hurricanes include, listed from the most recent to older events:

Hurricane Ida (2021) was a Category 4 storm at landfall near Port Fourchon, Louisiana, on August 29, 2021. By the time it reached Mississippi, it had weakened to a Category 1 hurricane. As Ida moved northeastward across Mississippi, it brought heavy rainfall and strong winds. The storm caused significant damage in coastal areas, including power outages, property damage, and flooding, particularly in southern Mississippi. Many communities faced disruptions due to power failures and damage to infrastructure.

Hurricane Katrina (2005), one of the most devastating hurricanes in U.S. history, made landfall as a Category 5 storm near New Orleans, Louisiana, on August 29, 2005, and weakened to a Category 3 hurricane as it crossed Mississippi. The impact on the Mississippi Gulf Coast was catastrophic, especially in cities like Biloxi and Gulfport. Katrina brought severe flooding, extensive wind damage, and the destruction of homes and businesses. The storm caused widespread devastation, with a significant storm surge that exacerbated the damage. The recovery and rebuilding efforts in the region have been extensive and ongoing.

Hurricane Camille (1969) struck the Mississippi Gulf Coast as a Category 5 storm on August 17, 1969, making landfall near Waveland, Mississippi. Camille was one of the most powerful hurricanes to hit the region, bringing massive storm surges and high winds. The hurricane caused severe flooding and widespread destruction, resulting in significant loss of life and extensive damage to infrastructure, homes, and businesses. Camille's impact on the Mississippi Gulf Coast remains a historic example of the power of hurricanes and the challenges of recovery.

Hurricane Betsy (1965) made landfall as a Category 4 storm on September 9, 1965, near the Louisiana-Mississippi border. The storm impacted the Mississippi Gulf Coast with significant flooding and wind damage. While less severe than Hurricane Camille, Betsy still caused notable damage and disruption in coastal areas. The hurricane's effects included property damage and interruptions to local communities, highlighting the vulnerability of the region to powerful storms.

Hurricane Audrey (1957) made landfall as a Category 4 hurricane on June 27, 1957, near the Texas-Louisiana border and weakened to a Category 3 storm as it moved into Mississippi. The hurricane brought substantial flooding and wind damage to the Mississippi

Gulf Coast. Audrey's impact resulted in significant property damage and disruptions to local communities, demonstrating the region's susceptibility to severe hurricanes.

2.3 Summary

Although the probability of a large-scale tsunami event in the GOM is low, this and previous studies have indicated that tsunami events with characteristics similar to those detailed in Horrillo et al. [2015] have the potential to cause severe flooding and damage to GOM coastal communities that is similar to or even greater than that seen from major hurricanes, particularly in open beach and barrier island regions. Tsunami hazard maritime products such as tsunami current magnitude, vorticity, safe/hazard zones would be central for future developments of maritime hazard maps, maritime emergency response as well as infrastructure planning. The results of this work are intended to provide guidance to local emergency managers to help with managing urban growth, evacuation planning, and public education with the vision to mitigate potential GOM tsunami hazards.

This report is organized as follows. Section 3 briefly describes all 9 landslide sources used for tsunami modeling (3.1) and the numerical models used for simulations (3.2). Section 4 covers the inundation and momentum flux maps for Mississippi. The comparison between tsunami inundation and hurricane storm surge inundation (tsunami inundation in terms of hurricane category) is given in Section 5 for the two new Gulf Coast communities. Current velocity and vorticity maps are described in Section 6 for the two new communities. ??? Section **??** presents a new CUDA meteotsunami model and the refined numerical results for a parameter study of GOM, with identification of coastal communities vulnerable to meteotsunami inundation.

3 Tsunami Inundation Modeling

3.1 Landslide Tsunami Sources

Nine large-scale landslide configurations were created assuming an unstable (gravity-driven) sediment deposit condition. Five of these landslide configurations are geological events identified by ten Brink et al. [2009b]: the Eastbreaks, Mississippi Canyon, and West Florida submarine landslides; and Chaytor et al. [2016]: the Yucatán #3 and Yucatán #5 landslides, which are shown as red hatched regions in Fig. 1. The Yucatán Shelf/Campeche Escarpment was the last remaining area of the GOM that had not been evaluated for landslide tsunami hazards, until high-resolution mapping data collected in 2013 [Paull et al., 2014] shows that the Yucatán Shelf/Campeche Escarpment margin has been subjected to intense modifications by Cenozoic mass wasting processes. Although no known tsunami events have been linked to these Yucatán sources, numerical modeling result shows that they are capable of generating tsunamis that could propagate throughout the GOM Basin [Chaytor et al., 2016]. The other four were obtained using a probabilistic methodology based on work by Maretzki et al. [2007] and Grilli et al. [2009] and extended for the GOM by Pampell-Manis et al. [2016]. The probabilistic landslide configurations were determined based on distributions of previous GOM submarine landslide dimensions through a Monte Carlo Simulation (MCS) approach. The MCS methodology incorporates a statistical correlation method for capturing trends seen in observational data for landslide size parameters while still allowing for randomness in the generated landslide dimensions. Slope stability analyses are performed for the MCS-generated trial landslide configurations using landslide and sediment properties and regional seismic loading (Peak Horizontal ground Acceleration, PHA) to determine landslide configurations which fail and produce a tsunami. The probability of each tsunamigenic failure is calculated based on the joint probability of the earthquake PHA and the probability that the trial landslide fails and produces a tsunami wave above a certain threshold. Those failures which produce the largest tsunami amplitude and have the highest probability of occurrence are deemed the most extreme probabilistic events, and the dimensions of these events are averaged to determine maximum credible probabilistic sources. The four maximum credible Probabilistic Submarine Landslides (PSLs) used as tsunami sources for this study are termed PSL-A, PSL-B1, PSL-B2, and PSL-C and are shown as blue hatched regions in Fig. 1. For a more complete discussion of GOM submarine landslide sources, the reader can consult Horrillo et al. [2015, 2018], Pampell-Manis et al. [2016].

Table 1: Submarine Landslide general information.

Submarine Landslide	Location (Lon, Lat)	Age/Recurrence (Years)	Area (km^2)	Volume (km^3)	Excavation Depth (m)	Modeled Volume (km^3)
East Breaks	-95.68, 27.70	$\sim 10000 - 25000$	~ 519.52	~ 21.95	~ 160	26.7
Mississippi	-90.00, 28.60	$\sim 7500 - 11000$	~ 3687.26	~ 425.54	~ 300	425
West Florida	-84.75, 25.95	> 10000	~ 647.57	~ 16.2	~ 150	18.4
Yucatán #3	-90.07, 23.00	–	~ 578	~ 38	~ 278	39.3
Yucatán #5	-89.80, 23.54	–	~ 1094	~ 70.2	~ 385	69.5
PSL-A	-94.30, 27.98	$\sim 7700 - 7800$	~ 1686	~ 57	~ 67	58
PSL-B1	-91.56, 28.05	$\sim 5400 - 5500$	~ 3118	~ 69	~ 44	57.3
PSL-B2	-91.01, 26.17	$\sim 4700 - 4800$	~ 282	~ 45	~ 323	68
PSL-C	-87.20, 28.62	$\sim 550 - 650$	~ 1529	~ 315	~ 404	357

3.2 Numerical Models

For the nine landslide tsunami sources considered here, tsunami wave development and subsequent propagation and inundation of coastal communities was modeled using coupled 3D and 2D numerical models [Horrillo et al., 2015]. The tsunami generation phase was modeled using the 3D model TSUNAMI3D [Horrillo, 2006, Horrillo et al., 2013], which solves the finite difference approximation of the full Navier-Stokes equations and the incompressibility (continuity) equation. Water and landslide material are represented as Newtonian fluids with different densities, and the landslide-water and water-air interfaces are tracked using the Volume of Fluid (VOF) method of Hirt and Nichols [1981], which is simplified to account for the large horizontal/vertical aspect ratio of the tsunami wave and the selected computational cell size required to construct an efficient 3D grid. The pressure term is split into hydrostatic and non-hydrostatic components. Although TSUNAMI3D has the capability of variable grids, the nesting capability necessary for modeling detailed inundation of coastal regions is too computationally intensive within the fully 3D model; thus, detailed inundation modeling is achieved by coupling the 3D model to a 2D model. Once the tsunami wave generated by the 3D model is fully developed, the wave is passed as an initial condition to the 2D model for modeling wave propagation and coastal inundation. The generated wave is considered fully developed when the total wave energy (potential plus kinetic) reaches a maximum and before the wave leaves the computational domain, as discussed in López-Venegas et al. [2015]. The 2D model used here is NEOWAVE [Yamazaki et al., 2008], a depth-integrated and non-hydrostatic model built on the nonlinear shallow water equations which includes a momentum-conserved advection scheme to model wave breaking and two-way nested grids for modeling higher-resolution wave runup and inundation. Propagation and inundation are calculated via a series of nested grids of increasing resolution, from 15 arcsecond (450 m) resolution for a domain encompassing the entire northern GOM (Fig. 1), to finer resolutions of 3 arcseconds (90 m, from NOAA NCEI Coastal Relief Models), 1 arcsecond (30 m), and 1/3 arcsecond (10 m, from NOAA NCEI Tsunami Inundation Digital Elevation Models [DEMs]) to model detailed inundation of the most populated/ inundation-prone areas of each coastal community. The 3 arcsecond (90 m) subdomains encompassing each coastal community studied here are shown by red rectangles in Fig. 1.

4 Tsunami Maps

Tsunami inundation depth and extent has been modeled for one selected coastal community: Mississippi. Inundation (flooding) is determined by subtracting land elevation from water elevation, and elevations used are in reference to the Mean High Water (MHW) tidal datum. For this study, the tsunami inundation depth/extent modeled for each community is the maximum-of-maximums (MOM) inundation, which is calculated as the maximum inundation depth from an ensemble of inundation depths produced by each of the nine tsunami sources considered. That is, once inundation in a community has been modeled for each of the nine sources, the overall maximum inundation depth in each computational grid cell is taken as the MOM tsunami inundation in that cell. This approach gives a worst-case scenario of estimated tsunami inundation for each coastal community.

In this section, the numerical results (inundation and momentum flux maps) for each landslide source are presented for Gulfport, MS (grid 4) and Pascagoula, MS (grid 5). The MOM inundation map from all sources and the maximum inundation map by source are also shown. A summary table of each location's numerical gauge (at an approximate water depth of 20 m) shows maximum wave amplitude and arrival time after each landslide failure.

4.1 Mississippi

Table 2: Maximum tsunami wave amplitude and corresponding arrival time after landslide failure at Gulfport, MS numerical wave gauge: 30°3' 26.4594"N, 88°34' 37.0092"W (Fig. 1), approximate water depth 20 m.

Tsunami Source	Maximum Wave Amplitude (m)	Arrival Time After Landslide Failure (hr)
East Breaks	0.42	3.0
PSL-A	0.46	2.6
PSL-B1	0.48	1.9
PSL-B2	0.52	2.1
Mississippi Canyon	3.68	1.2
PSL-C	3.31	1.3
West Florida	0.40	2.1
Yucatán #3	1.12	2.3
Yucatán #5	0.58	2.4

Mississippi
East Breaks submarine landslide
Maximum Momentum Flux

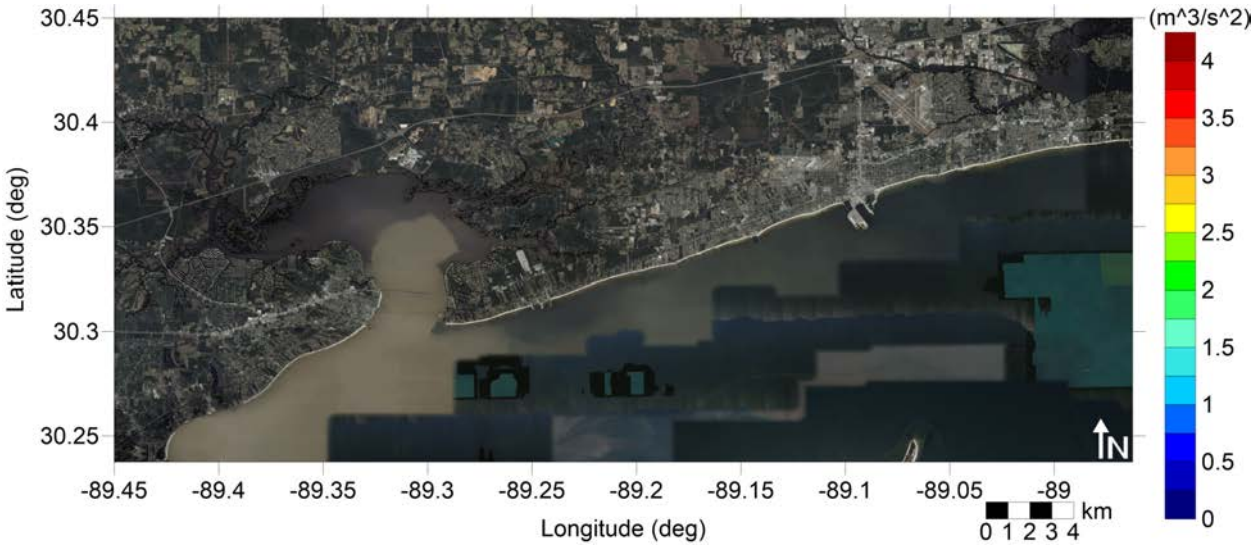

Figure 2: Maximum momentum flux (m^3/s^2) caused by the East Breaks submarine landslide in Gulfport, MS. Arrows represent direction of maximum momentum flux. Contour drawn is the zero-meter contour for land elevation.

Mississippi
East Breaks submarine landslide
Maximum Momentum Flux

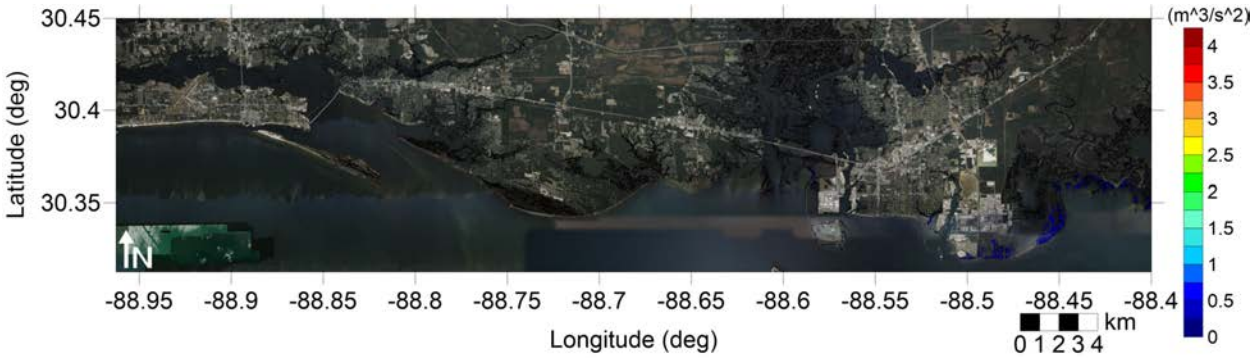

Figure 3: Maximum momentum flux (m^3/s^2) caused by the East Breaks submarine landslide in Pascagoula, MS. Arrows represent direction of maximum momentum flux. Contour drawn is the zero-meter contour for land elevation.

Mississippi
East Breaks submarine landslide
Maximum Inundation Depth

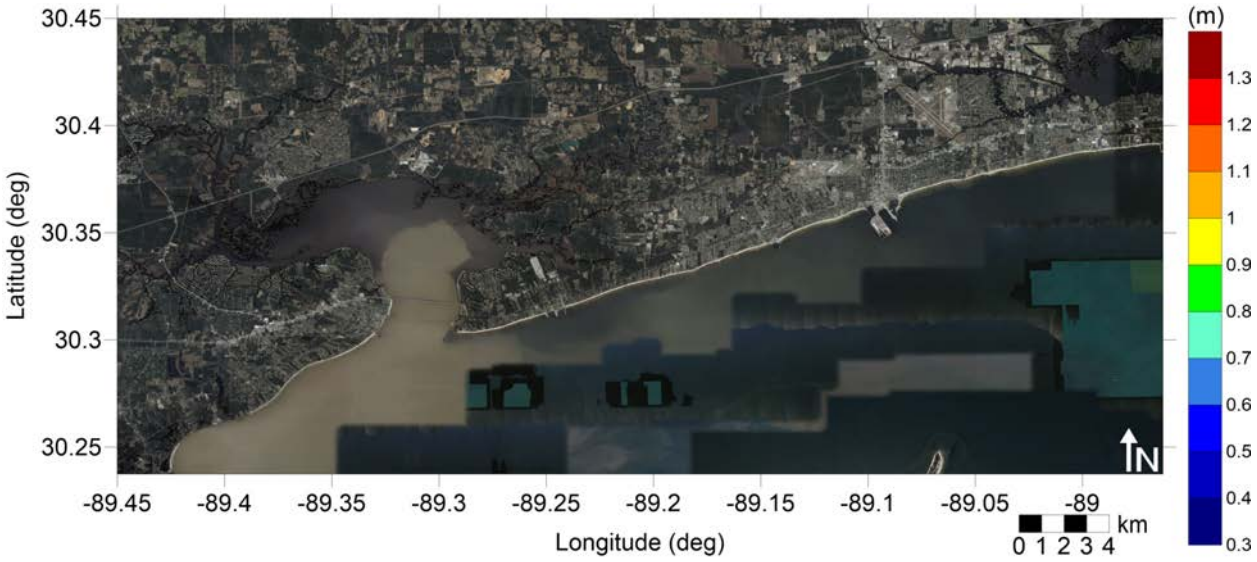

Figure 4: Maximum inundation depth (m) caused by the East Breaks submarine landslide in Gulfport, MS. Contour drawn is the zero-meter contour for land elevation.

Mississippi
East Breaks submarine landslide
Maximum Inundation Depth

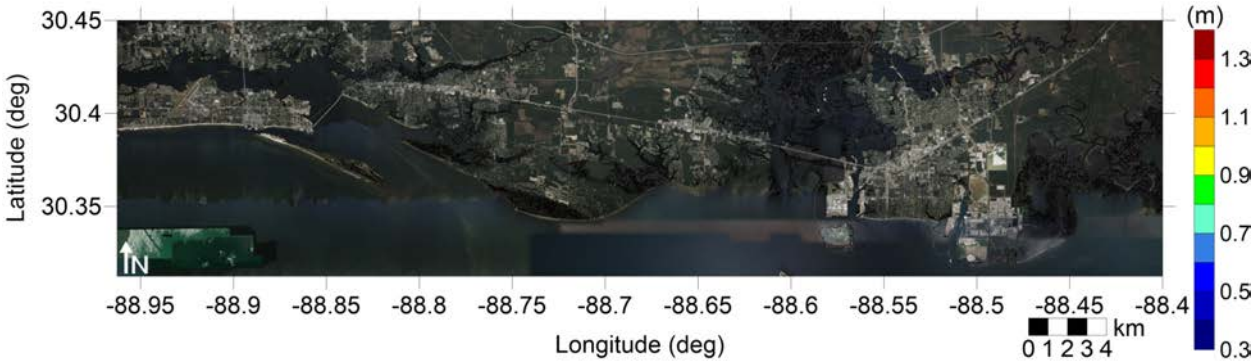

Figure 5: Maximum inundation depth (m) caused by the East Breaks submarine landslide in Pascagoula, MS. Contour drawn is the zero-meter contour for land elevation.

Mississippi
Probabilistic Submarine Landslide A
Maximum Momentum Flux

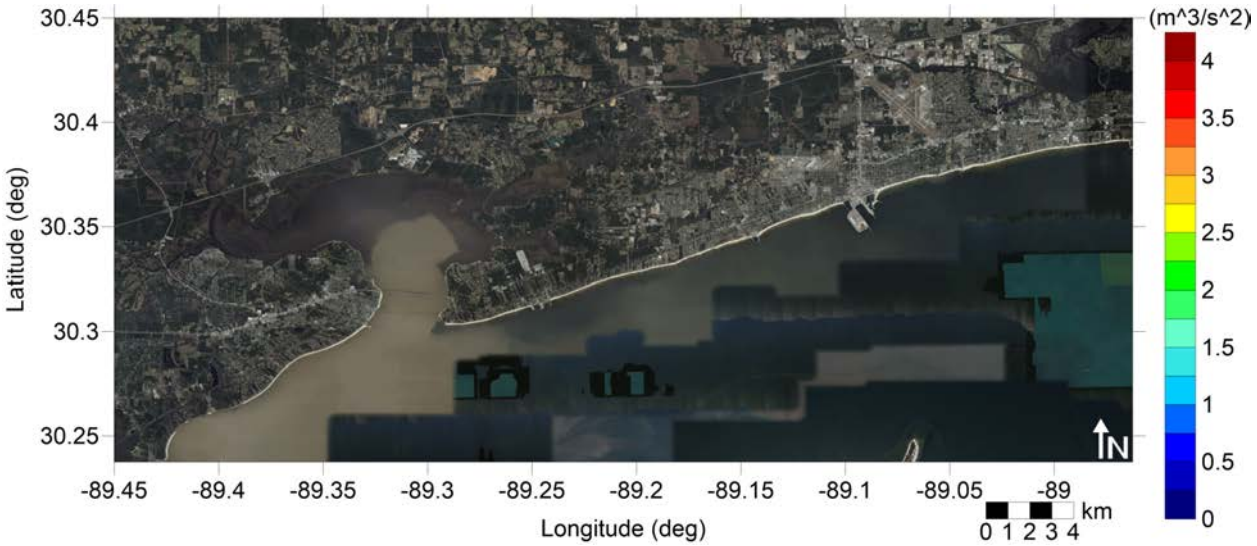

Figure 6: Maximum momentum flux (m^3/s^2) caused by the Probabilistic Submarine Landslide A in Gulfport, MS. Arrows represent direction of maximum momentum flux. Contour drawn is the zero-meter contour for land elevation.

Mississippi
Probabilistic Submarine Landslide A
Maximum Momentum Flux

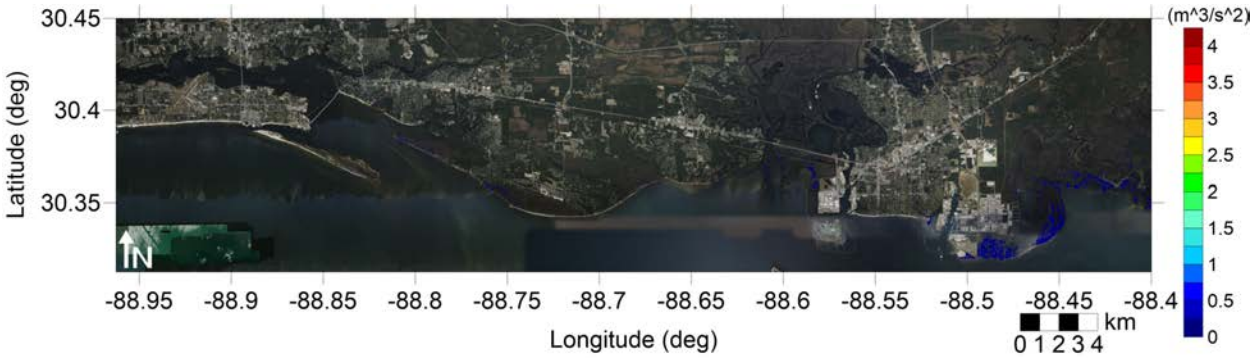

Figure 7: Maximum momentum flux (m^3/s^2) caused by the Probabilistic Submarine Landslide A in Pascagoula, MS. Arrows represent direction of maximum momentum flux. Contour drawn is the zero-meter contour for land elevation.

Mississippi
Probabilistic Submarine Landslide A
Maximum Inundation Depth

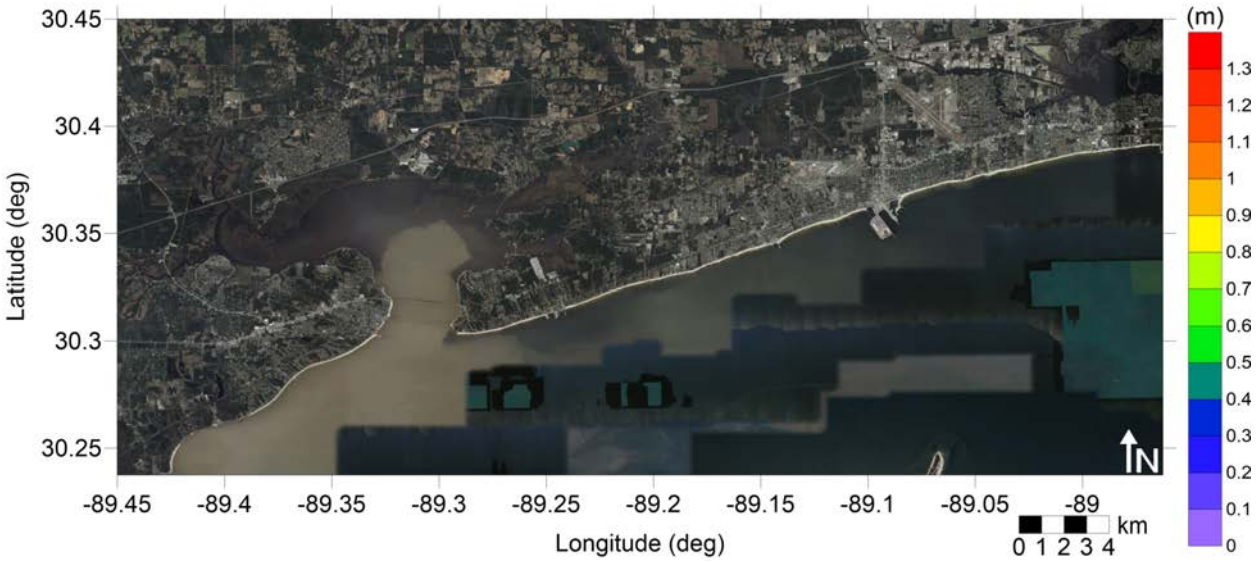

Figure 8: Maximum inundation depth (m) caused by the Probabilistic Submarine Landslide A in Gulfport, MS. Contour drawn is the zero-meter contour for land elevation.

Mississippi
Probabilistic Submarine Landslide A
Maximum Inundation Depth

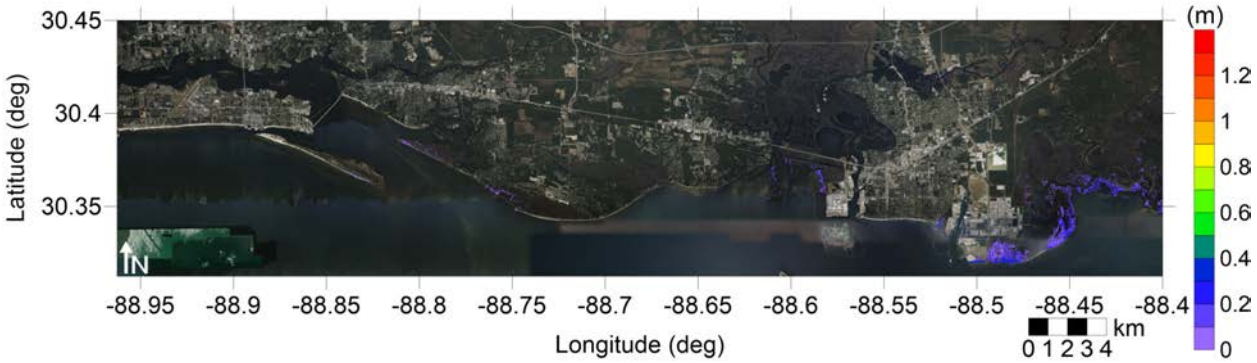

Figure 9: Maximum inundation depth (m) caused by the Probabilistic Submarine Landslide A in Pascagoula, MS. Contour drawn is the zero-meter contour for land elevation.

Mississippi
Probabilistic Submarine Landslide B1
Maximum Momentum Flux

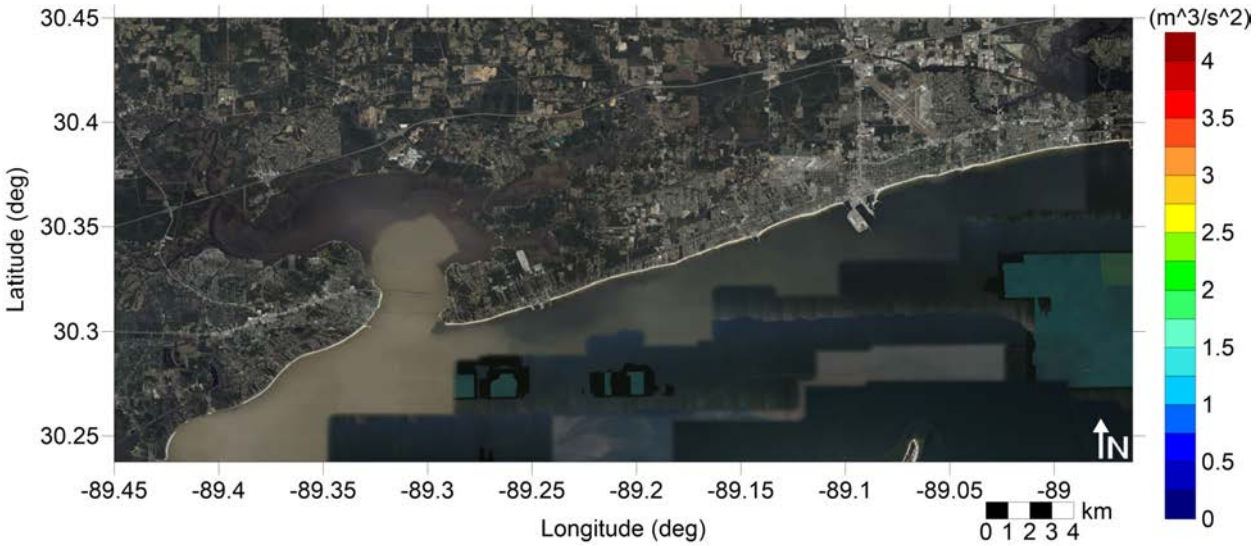

Figure 10: Maximum momentum flux (m^3/s^2) caused by the Probabilistic Submarine Landslide B1 in Gulfport, MS. Arrows represent direction of maximum momentum flux. Contour drawn is the zero-meter contour for land elevation.

Mississippi
Probabilistic Submarine Landslide B1
Maximum Momentum Flux

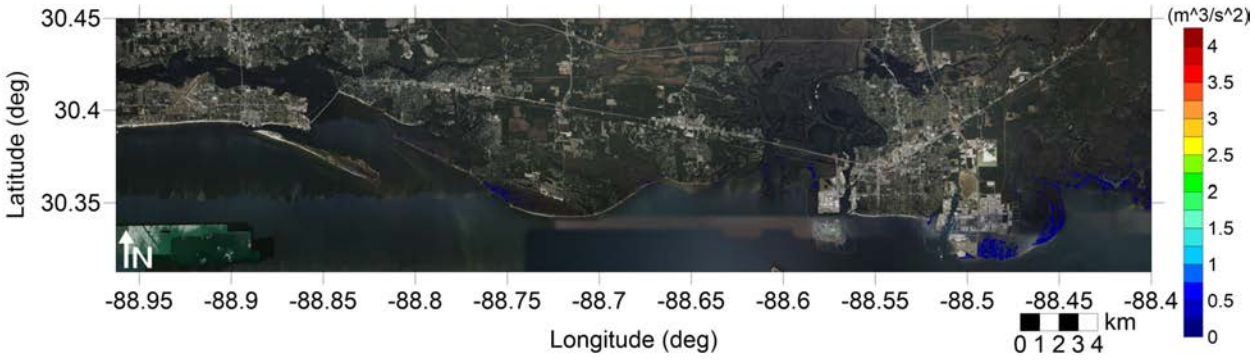

Figure 11: Maximum momentum flux (m^3/s^2) caused by the Probabilistic Submarine Landslide B1 in Pascagoula, MS. Arrows represent direction of maximum momentum flux. Contour drawn is the zero-meter contour for land elevation.

Mississippi
Probabilistic Submarine Landslide B1
Maximum Inundation Depth

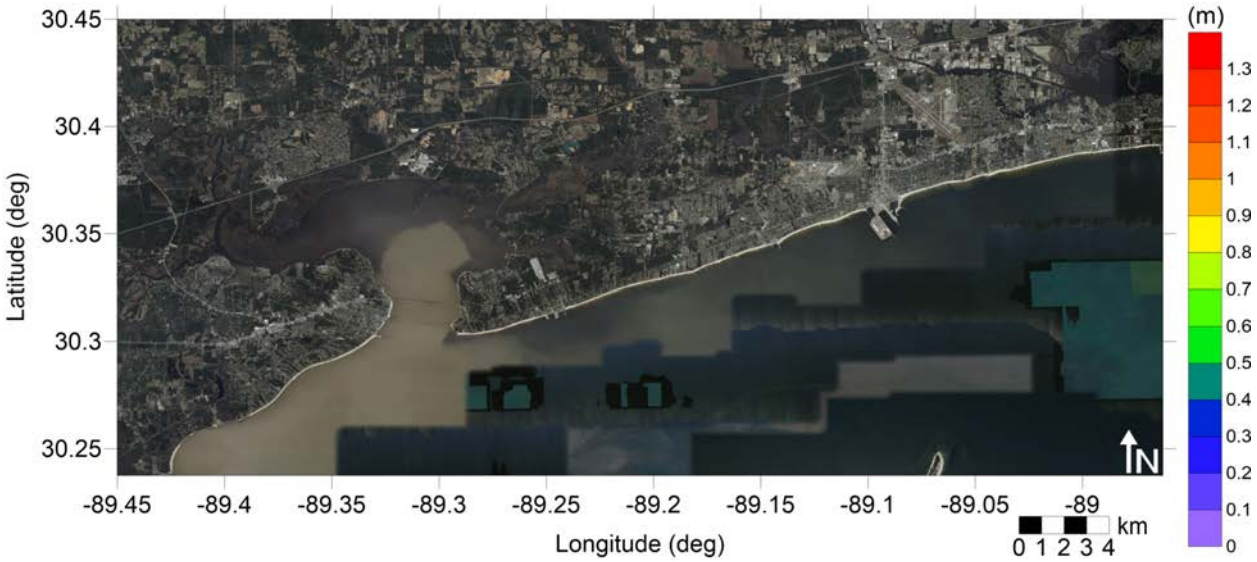

Figure 12: Maximum inundation depth (m) caused by the Probabilistic Submarine Landslide B1 in Gulfport, MS. Contour drawn is the zero-meter contour for land elevation.

Mississippi
Probabilistic Submarine Landslide B1
Maximum Inundation Depth

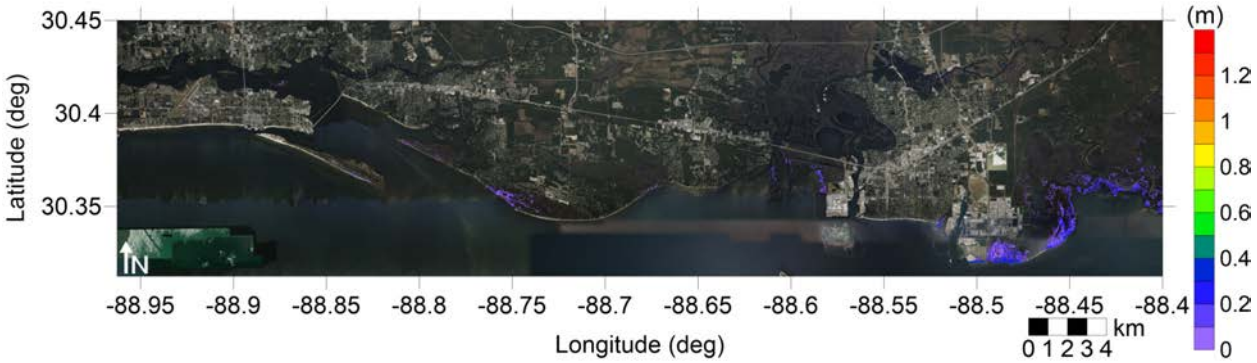

Figure 13: Maximum inundation depth (m) caused by the Probabilistic Submarine Landslide B1 in Pascagoula, MS. Contour drawn is the zero-meter contour for land elevation.

Mississippi
Probabilistic Submarine Landslide B2
Maximum Momentum Flux

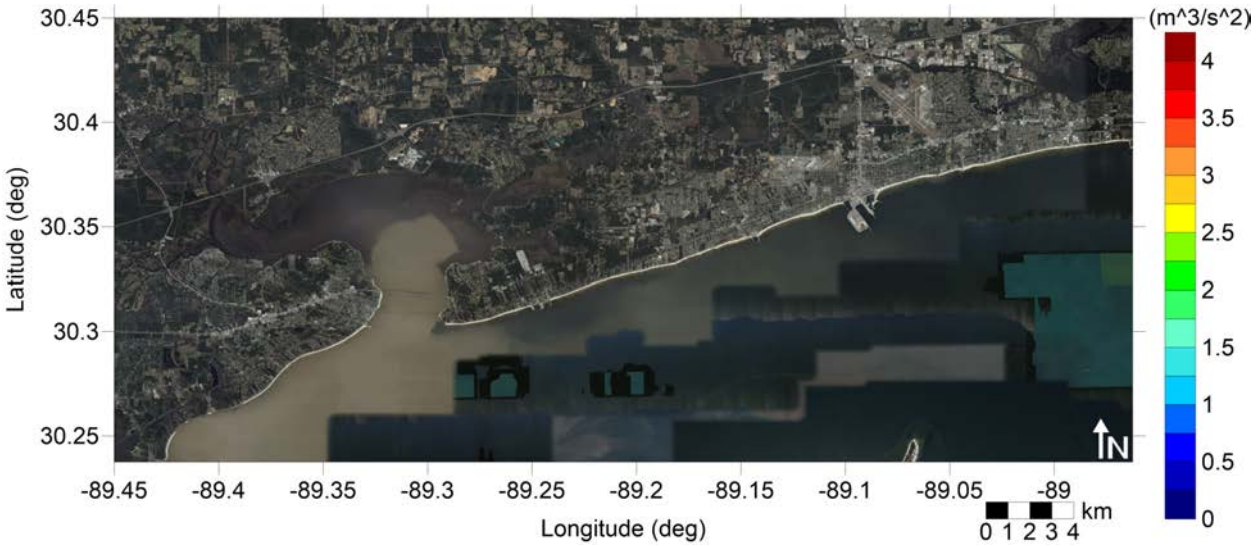

Figure 14: Maximum momentum flux (m^3/s^2) caused by the Probabilistic Submarine Landslide B2 in Gulfport, MS. Arrows represent direction of maximum momentum flux. Contour drawn is the zero-meter contour for land elevation.

Mississippi
Probabilistic Submarine Landslide B2
Maximum Momentum Flux

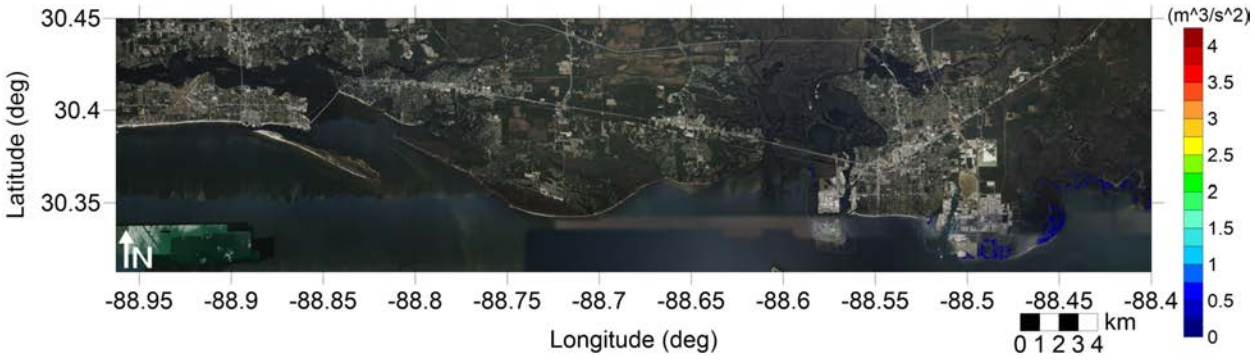

Figure 15: Maximum momentum flux (m^3/s^2) caused by the Probabilistic Submarine Landslide B2 in Pascagoula, MS. Arrows represent direction of maximum momentum flux. Contour drawn is the zero-meter contour for land elevation.

Mississippi
Probabilistic Submarine Landslide B2
Maximum Inundation Depth

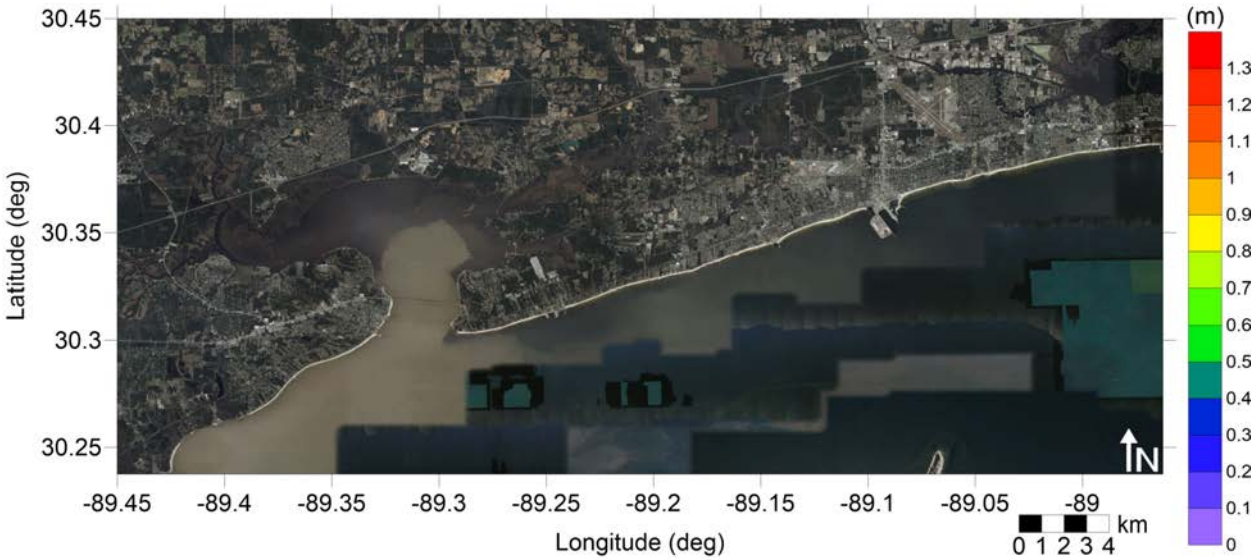

Figure 16: Maximum inundation depth (m) caused by the Probabilistic Submarine Landslide B2 in Gulfport, MS. Contour drawn is the zero-meter contour for land elevation.

Mississippi
Probabilistic Submarine Landslide B2
Maximum Inundation Depth

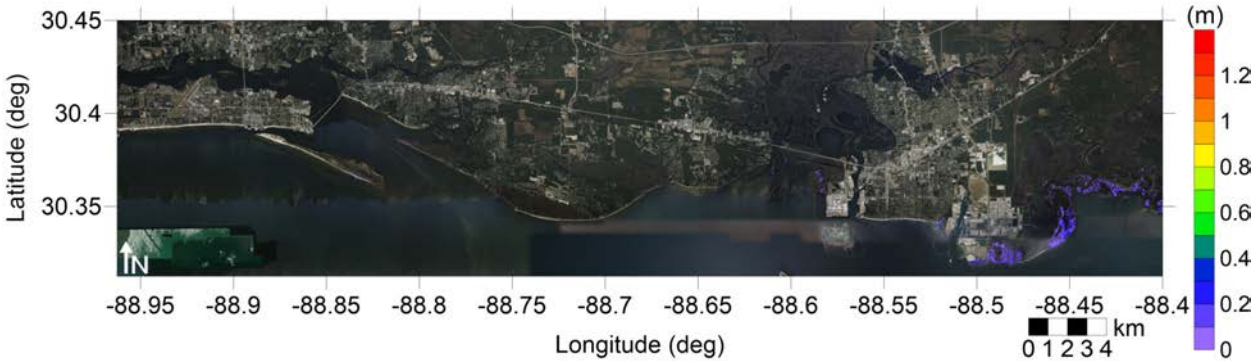

Figure 17: Maximum inundation depth (m) caused by the Probabilistic Submarine Landslide B2 in Pascagoula, MS. Contour drawn is the zero-meter contour for land elevation.

Mississippi
Mississippi Canyon submarine landslide
Maximum Momentum Flux

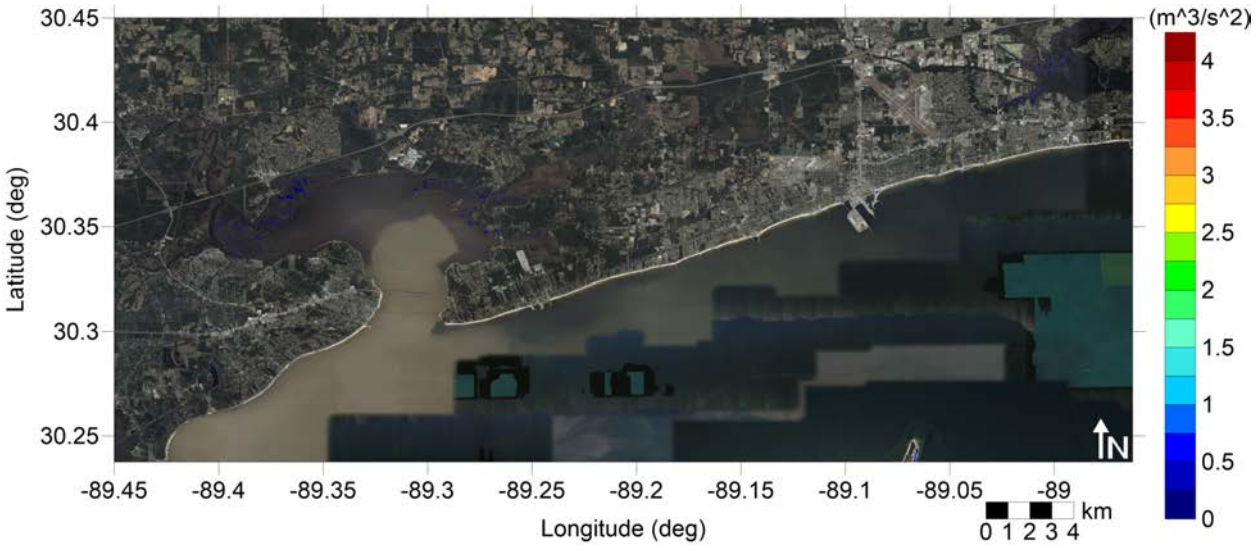

Figure 18: Maximum momentum flux (m^3/s^2) caused by the Mississippi Canyon submarine landslide in Gulfport, MS. Arrows represent direction of maximum momentum flux. Contour drawn is the zero-meter contour for land elevation.

Mississippi
Mississippi Canyon submarine landslide
Maximum Momentum Flux

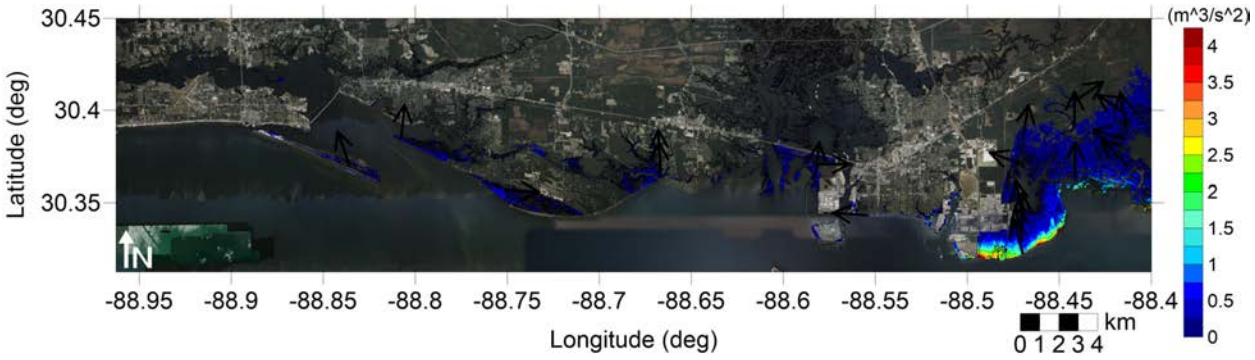

Figure 19: Maximum momentum flux (m^3/s^2) caused by the Mississippi Canyon submarine landslide in Pascagoula, MS. Arrows represent direction of maximum momentum flux. Contour drawn is the zero-meter contour for land elevation.

Mississippi
Mississippi Canyon submarine landslide
Maximum Inundation Depth

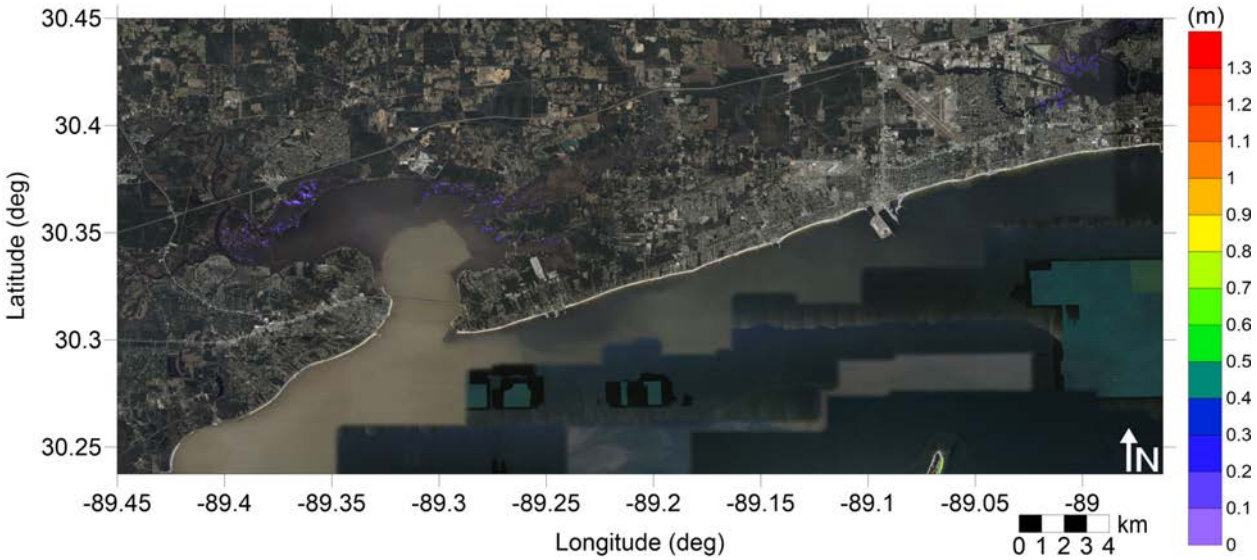

Figure 20: Maximum inundation depth (m) caused by the Mississippi Canyon submarine landslide in Gulfport, MS. Contour drawn is the zero-meter contour for land elevation.

Mississippi
Mississippi Canyon submarine landslide
Maximum Inundation Depth

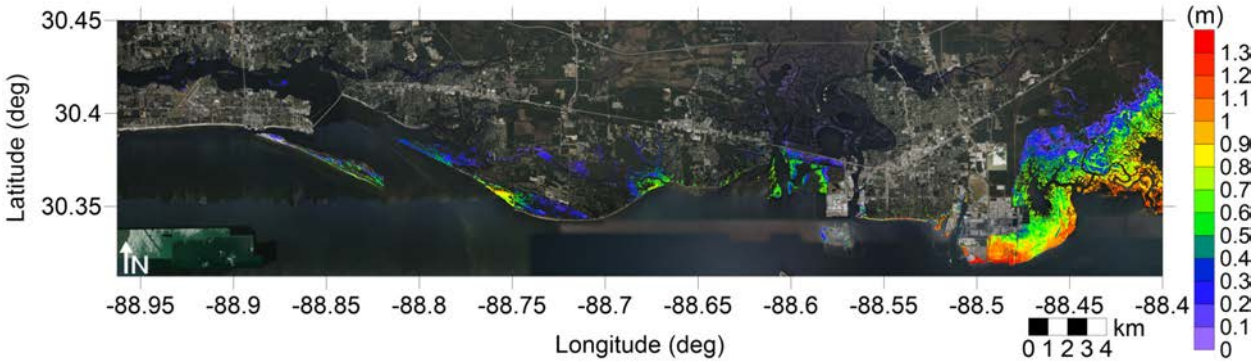

Figure 21: Maximum inundation depth (m) caused by the Mississippi Canyon submarine landslide in Pascagoula, MS. Contour drawn is the zero-meter contour for land elevation.

Mississippi
Probabilistic Submarine Landslide C
Maximum Momentum Flux

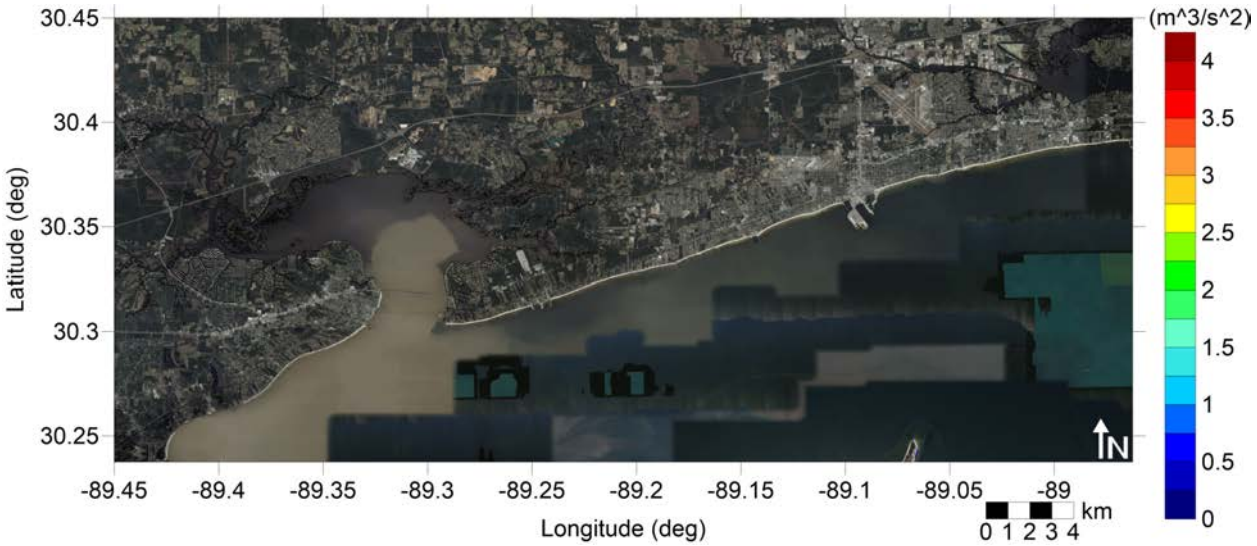

Figure 22: Maximum momentum flux (m^3/s^2) caused by the Probabilistic Submarine Landslide C in Gulfport, MS. Arrows represent direction of maximum momentum flux. Contour drawn is the zero-meter contour for land elevation.

Mississippi
Probabilistic Submarine Landslide C
Maximum Momentum Flux

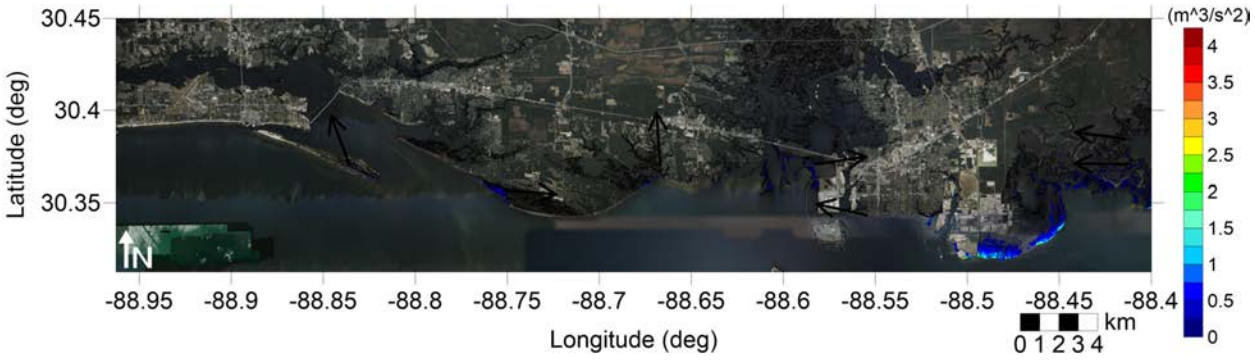

Figure 23: Maximum momentum flux (m^3/s^2) caused by the Probabilistic Submarine Landslide C in Pascagoula, MS. Arrows represent direction of maximum momentum flux. Contour drawn is the zero-meter contour for land elevation.

Mississippi
Probabilistic Submarine Landslide C
Maximum Inundation Depth

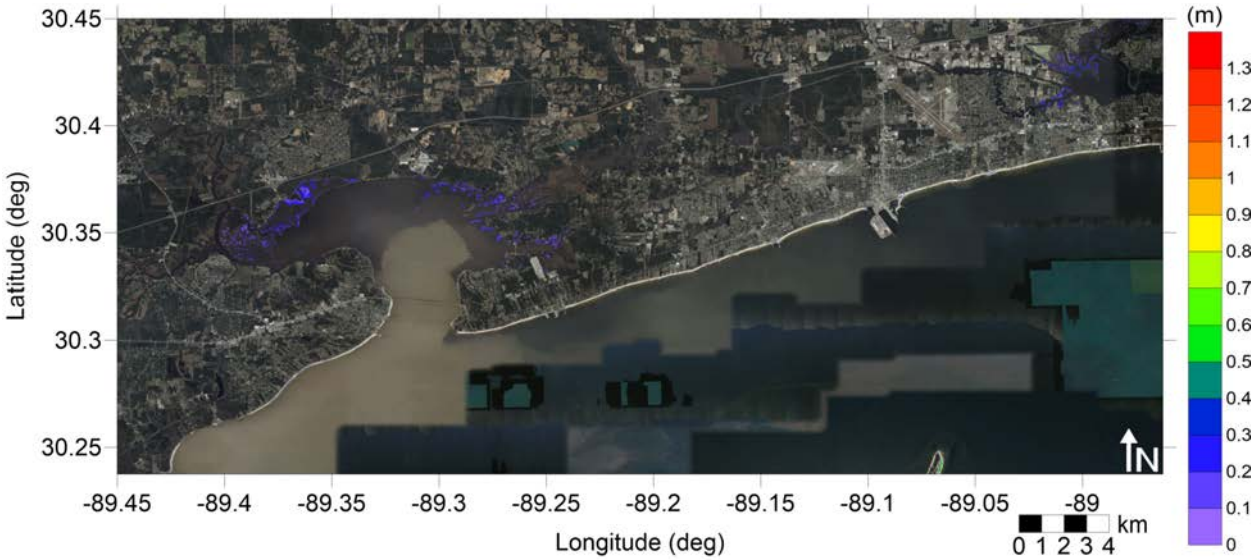

Figure 24: Maximum inundation depth (m) caused by the Probabilistic Submarine Landslide C in Gulfport, MS. Contour drawn is the zero-meter contour for land elevation.

Mississippi
Probabilistic Submarine Landslide C
Maximum Inundation Depth

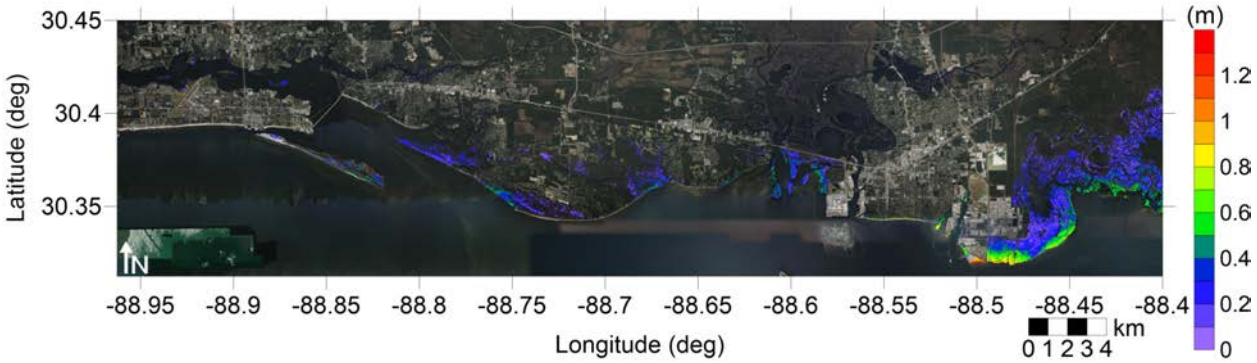

Figure 25: Maximum inundation depth (m) caused by the Probabilistic Submarine Landslide C in Pascagoula, MS. Contour drawn is the zero-meter contour for land elevation.

Mississippi
West Florida submarine landslide
Maximum Momentum Flux

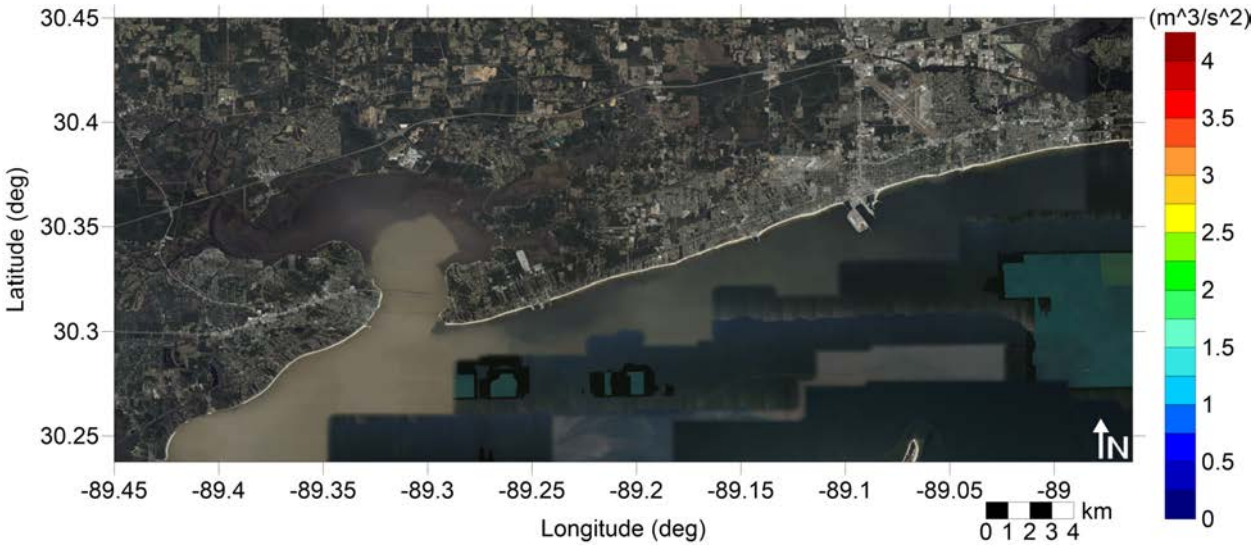

Figure 26: Maximum momentum flux (m^3/s^2) caused by the West Florida submarine landslide in Gulfport, MS. Arrows represent direction of maximum momentum flux. Contour drawn is the zero-meter contour for land elevation.

Mississippi
West Florida submarine landslide
Maximum Momentum Flux

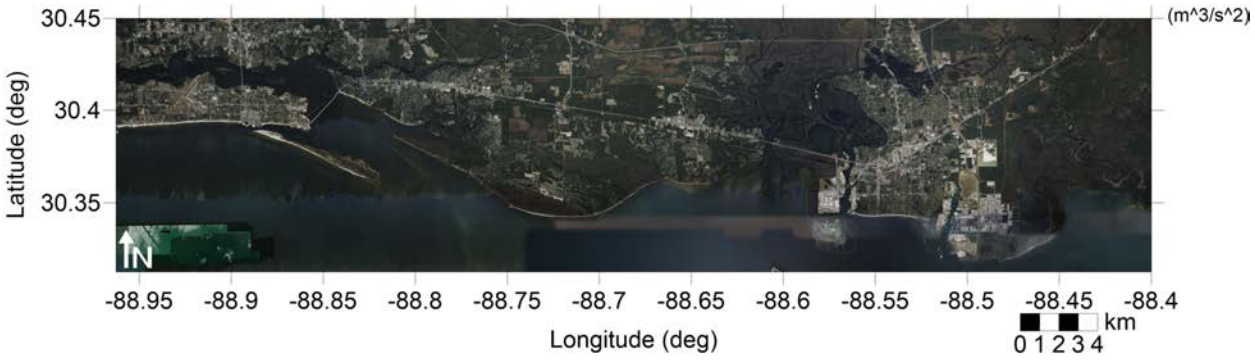

Figure 27: Maximum momentum flux (m^3/s^2) caused by the West Florida submarine landslide in Pascagoula, MS. Arrows represent direction of maximum momentum flux. Contour drawn is the zero-meter contour for land elevation.

Mississippi
West Florida submarine landslide
Maximum Inundation Depth

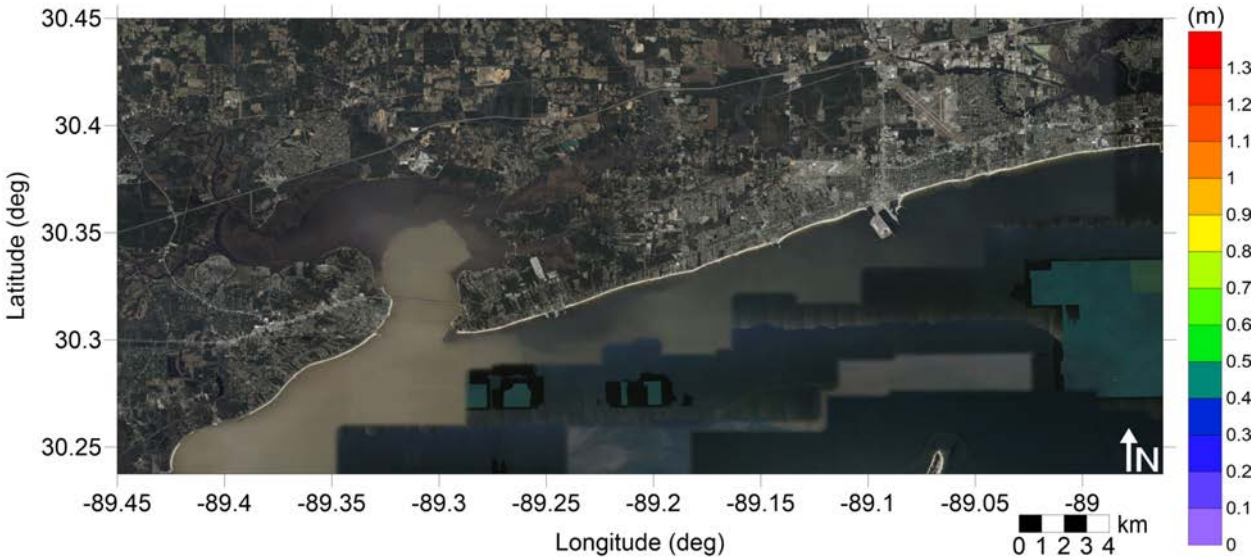

Figure 28: Maximum inundation depth (m) caused by the West Florida submarine landslide in Gulfport, MS. Contour drawn is the zero-meter contour for land elevation.

Mississippi
West Florida submarine landslide
Maximum Inundation Depth

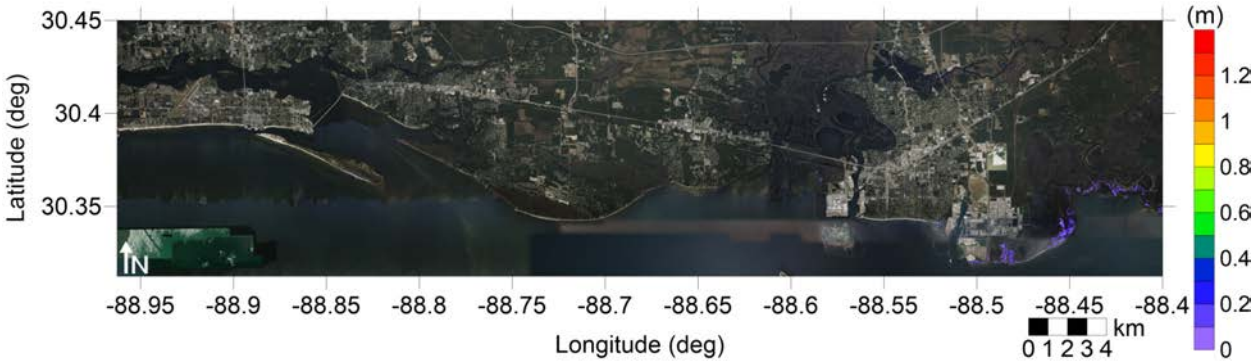

Figure 29: Maximum inundation depth (m) caused by the West Florida submarine landslide in Pascagoula, MS. Contour drawn is the zero-meter contour for land elevation.

Mississippi
Yucatán 3 submarine landslide
Maximum Momentum Flux

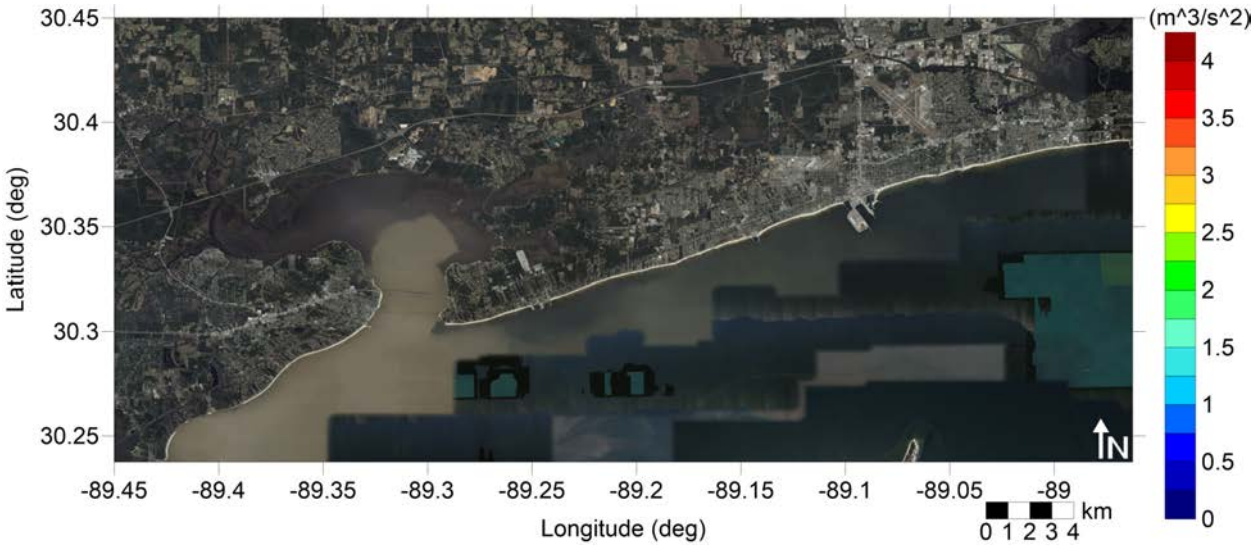

Figure 30: Maximum momentum flux (m^3/s^2) caused by the Yucatán 3 submarine landslide in Gulfport, MS. Arrows represent direction of maximum momentum flux. Contour drawn is the zero-meter contour for land elevation.

Mississippi
Yucatán 3 submarine landslide
Maximum Momentum Flux

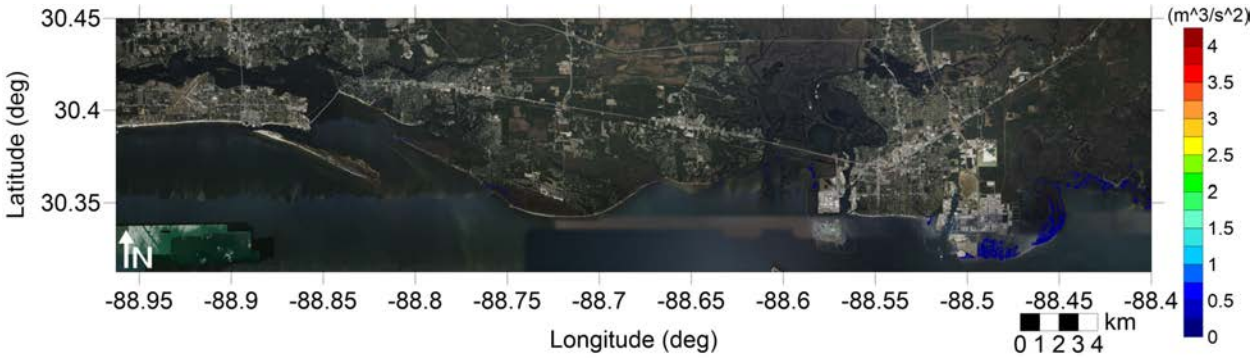

Figure 31: Maximum momentum flux (m^3/s^2) caused by the Yucatán 3 submarine landslide in Pascagoula, MS. Arrows represent direction of maximum momentum flux. Contour drawn is the zero-meter contour for land elevation.

Mississippi
Yucatán 3 submarine landslide
Maximum Inundation Depth

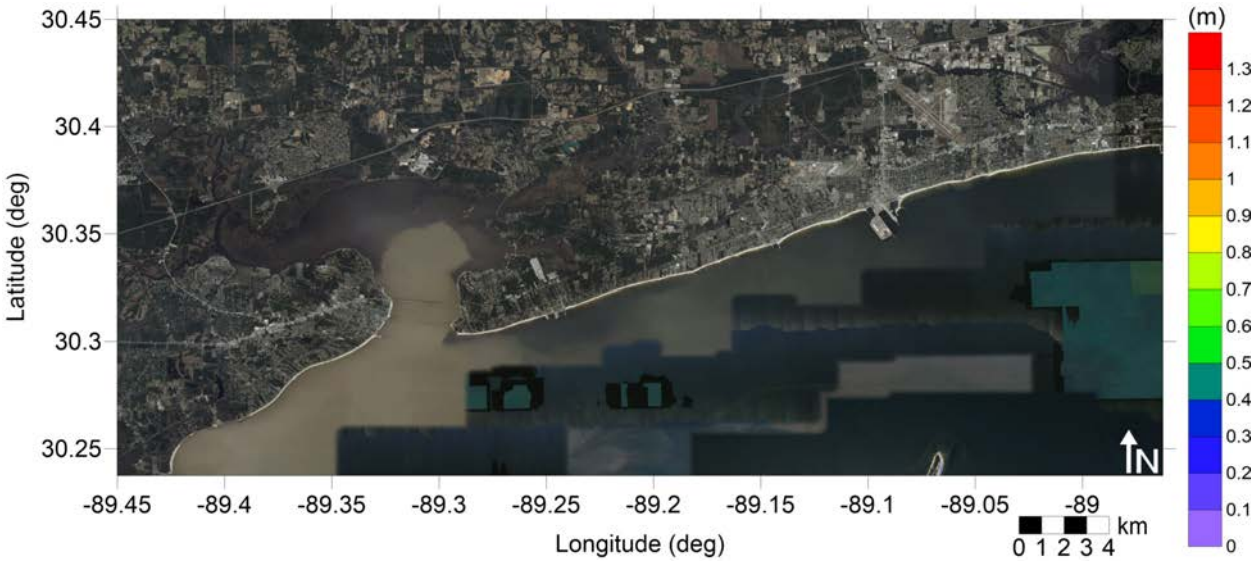

Figure 32: Maximum inundation depth (m) caused by the Yucatán 3 submarine landslide in Gulfport, MS. Contour drawn is the zero-meter contour for land elevation.

Mississippi
Yucatán 3 submarine landslide
Maximum Inundation Depth

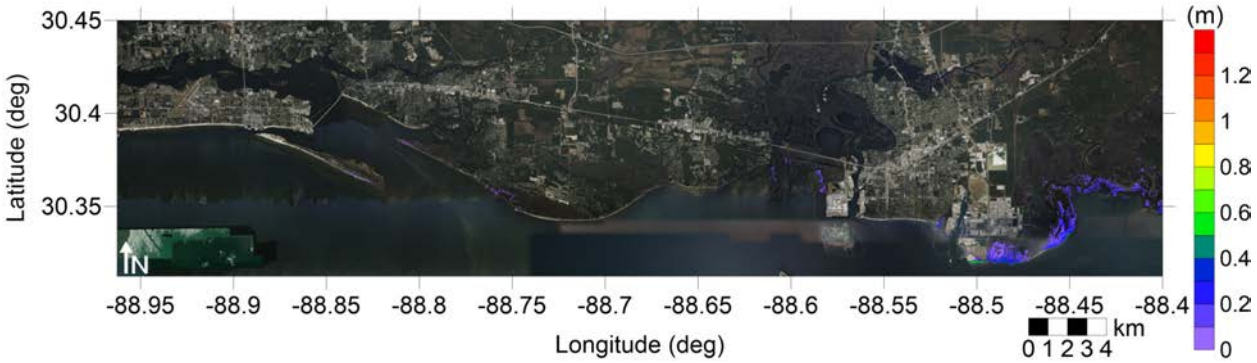

Figure 33: Maximum inundation depth (m) caused by the Yucatán 3 submarine landslide in Pascagoula, MS. Contour drawn is the zero-meter contour for land elevation.

Mississippi
Yucatán 5 submarine landslide
Maximum Momentum Flux

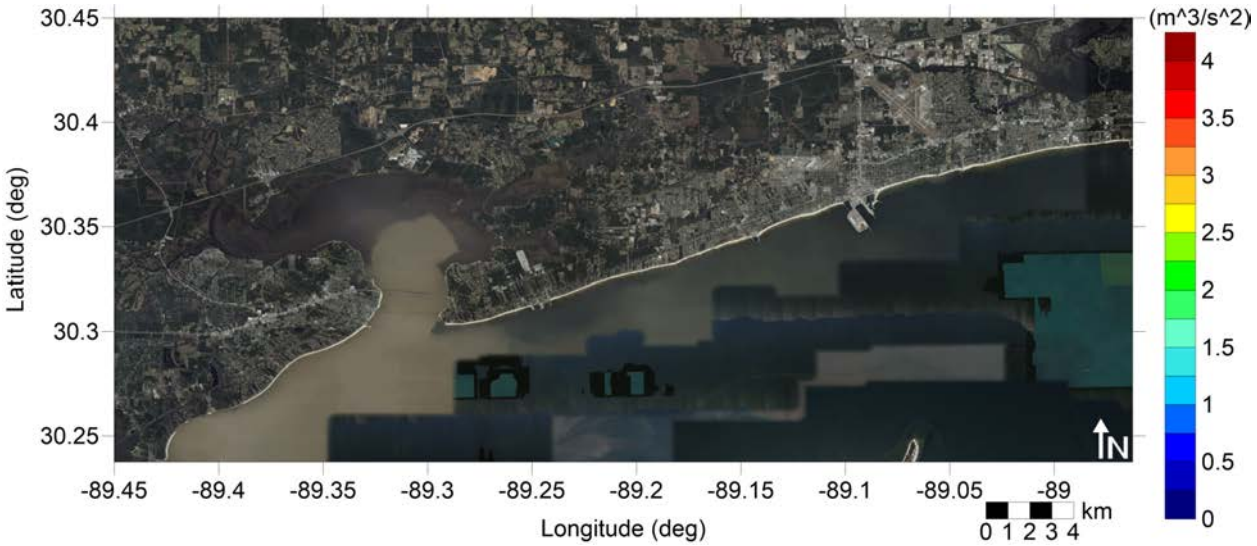

Figure 34: Maximum momentum flux (m^3/s^2) caused by the Yucatán 5 submarine landslide in Gulfport, MS. Arrows represent direction of maximum momentum flux. Contour drawn is the zero-meter contour for land elevation.

Mississippi
Yucatán 5 submarine landslide
Maximum Momentum Flux

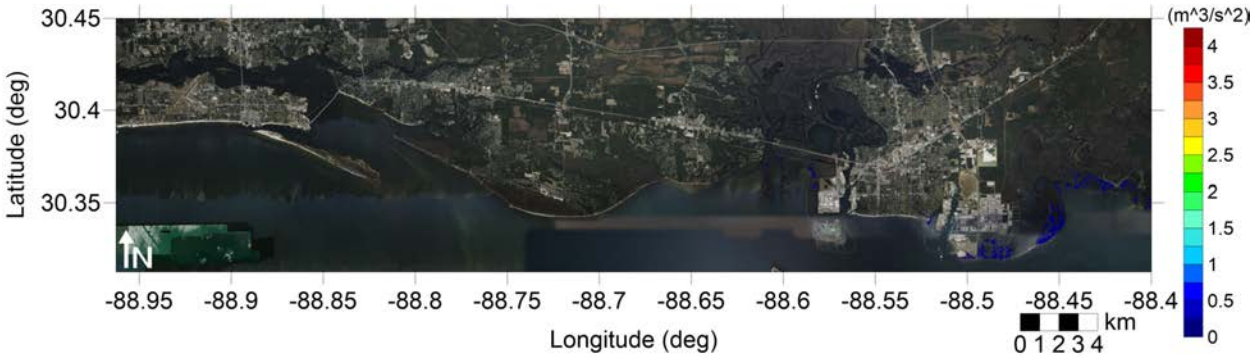

Figure 35: Maximum momentum flux (m^3/s^2) caused by the Yucatán 5 submarine landslide in Pascagoula, MS. Arrows represent direction of maximum momentum flux. Contour drawn is the zero-meter contour for land elevation.

Mississippi
Yucatán 5 submarine landslide
Maximum Inundation Depth

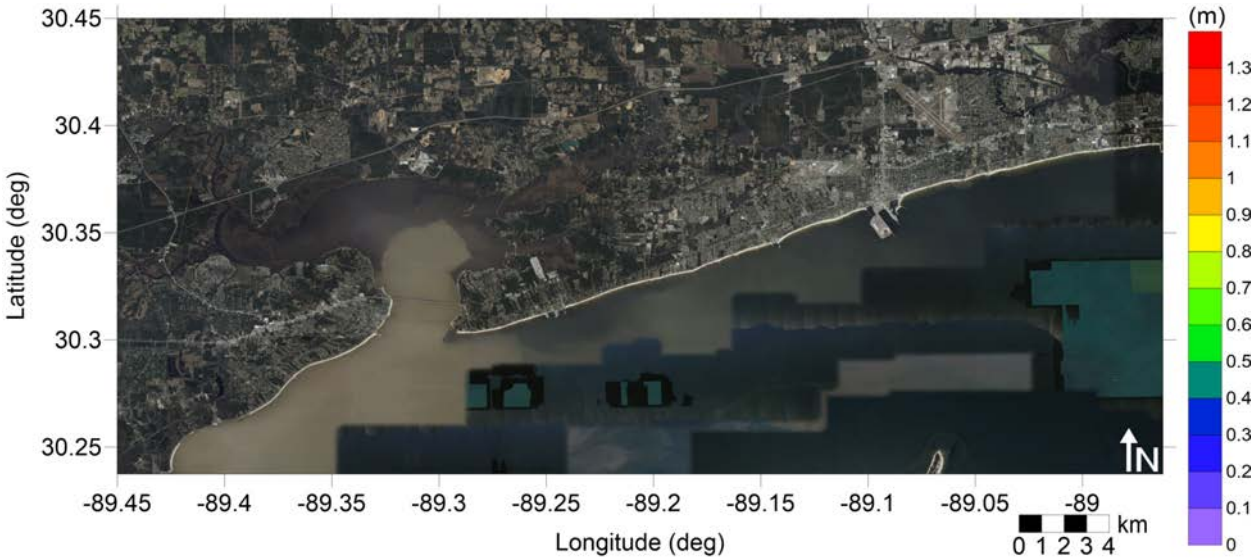

Figure 36: Maximum inundation depth (m) caused by the Yucatán 5 submarine landslide in Gulfport, MS. Contour drawn is the zero-meter contour for land elevation.

Mississippi
Yucatán 5 submarine landslide
Maximum Inundation Depth

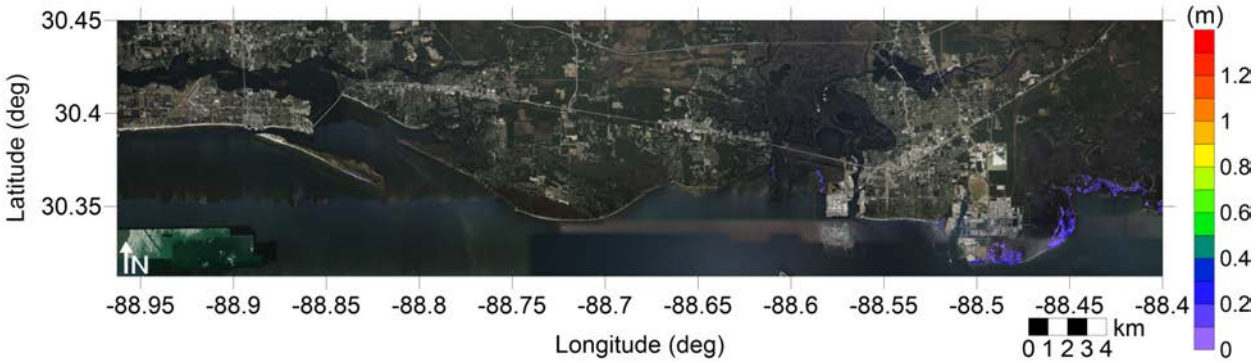

Figure 37: Maximum inundation depth (m) caused by the Yucatán 5 submarine landslide in Pascagoula, MS. Contour drawn is the zero-meter contour for land elevation.

Mississippi
All Sources
Maximum of Maximum Inundation Depth

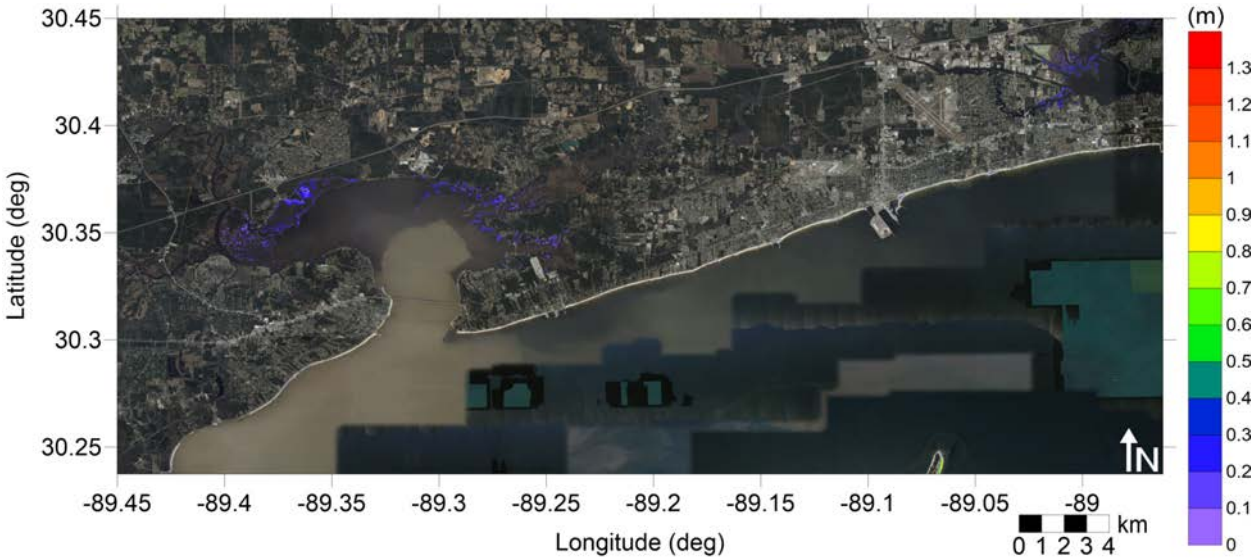

Figure 38: Maximum of maximums inundation depth (m) in Gulfport, MS, calculated as the maximum inundation depth in each grid cell from an ensemble of all tsunami sources considered. Contour drawn is the zero-meter contour for land elevation.

Mississippi
All Sources
Maximum of Maximum Inundation Depth

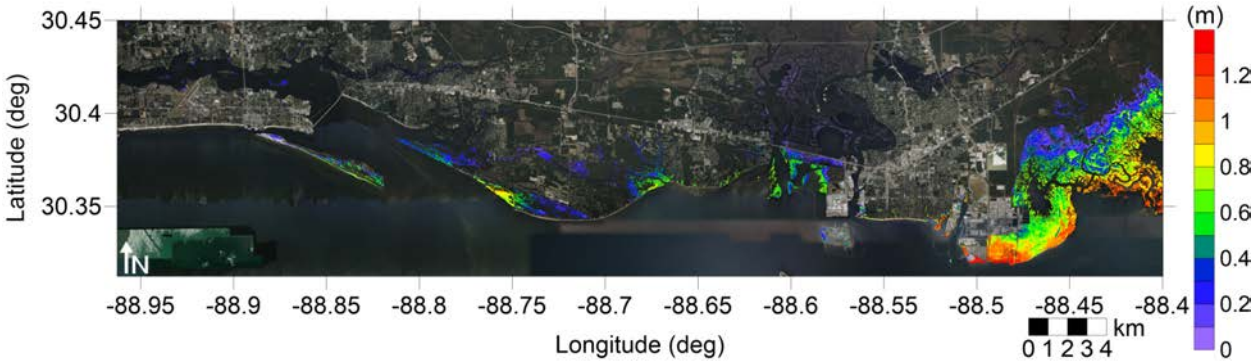

Figure 39: Maximum of maximums inundation depth (m) in Pascagoula, MS, calculated as the maximum inundation depth in each grid cell from an ensemble of all tsunami sources considered. Contour drawn is the zero-meter contour for land elevation.

Mississippi
All Sources
Maximum Inundation Depth by Source

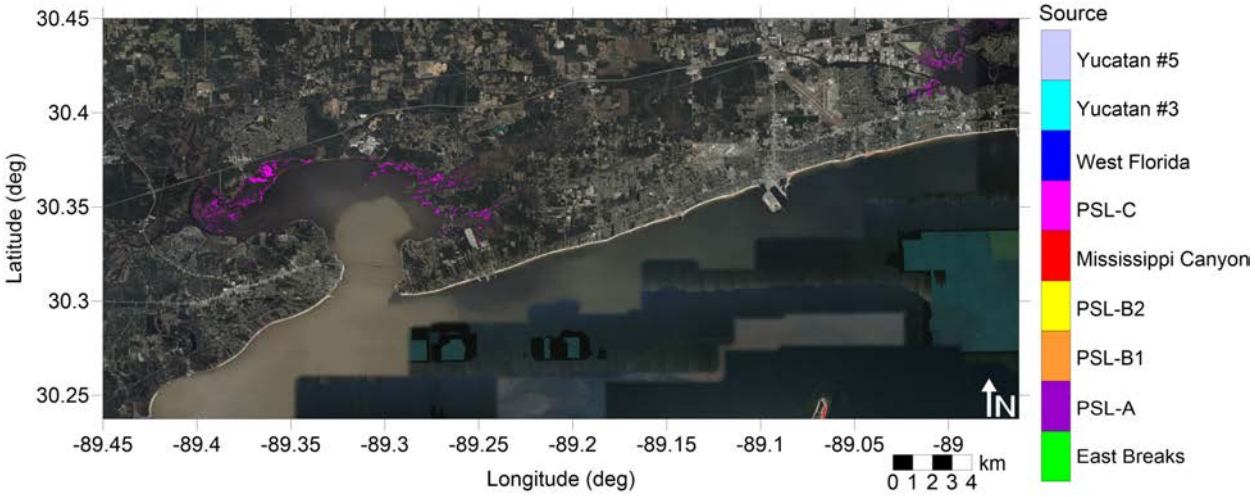

Figure 40: Indication of the tsunami source which causes the maximum of maximums inundation depth (m) in each grid cell from an ensemble of all tsunami sources in Gulfport, MS. Contour drawn is the zero-meter contour for land elevation.

Mississippi
All Sources
Maximum Inundation Depth by Source

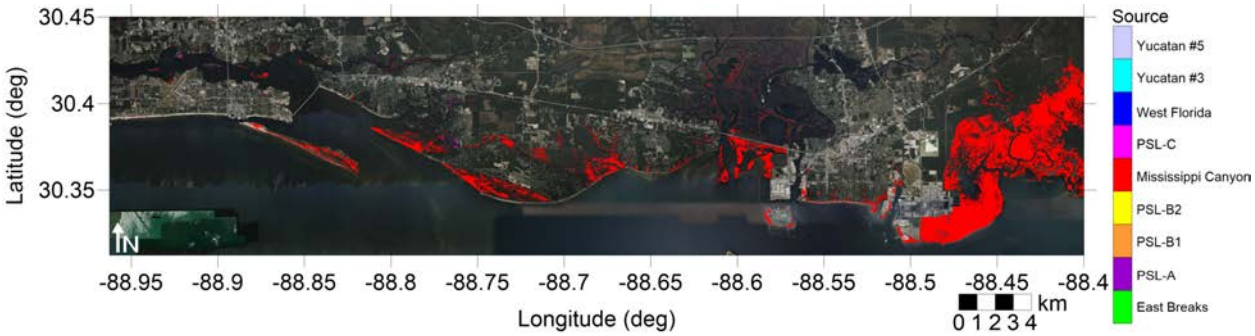

Figure 41: Indication of the tsunami source which causes the maximum of maximums inundation depth (m) in each grid cell from an ensemble of all tsunami sources in Pascagoula, MS. Contour drawn is the zero-meter contour for land elevation.

5 Tsunami and Hurricane Storm Surge Inundation

Due to the limitations on availability of high-resolution (1/3 arcsecond) DEMs, detailed inundation maps for all communities along the Gulf Coast are not yet possible. In an effort to develop a first-order estimate of potential tsunami inundation for those locations where detailed inundation maps have not yet been developed, we compare tsunami inundation modeled for the communities mentioned above to hurricane storm surge modeled data. The motivation for and implications of this approach are twofold. It provides a way to assess tsunami inundation in unmapped communities based on existing storm surge flood data and also relates the level of tsunami hazard to that of another hazard that is better defined in this region. Tsunamis are not well-understood as a threat along the Gulf Coast, making tsunami hazard mitigation efforts somewhat difficult. However, hurricane is a relatively well-understood threat in this region, and hurricane preparedness approaches are well-developed. As a result, comparisons of tsunami and hurricane storm surge inundation levels provide a more understandable and accessible idea of the level of hazard presented by potential tsunami events and can serve as a basis for tsunami preparedness efforts.

The hurricane storm surge data used here is available from the Sea, Lake, and Overland Surges from Hurricanes (SLOSH) model (http://www.nhc.noaa.gov/surge/slosh.php). The SLOSH model was developed by the National Weather Service (NWS) to provide estimates of storm surge heights caused by historical, predicted, or hypothetical hurricanes based on different values for atmospheric pressure, hurricane size, forward speed, and track. It uses a polar, elliptical, or hyperbolic grid for computations, leading to higher resolutions near coastal areas of interest. Some limitations of the SLOSH model should be acknowledged. Resolution of the model varies from tens of meters to a kilometer or more. Near the coastal communities of interest here, resolution is on the order of 1 km. Sub-grid scale water and topographic features such as channels, rivers, levees, and roads, are parameterized instead of being explicitly modeled. Despite these limitations, the hurricane storm surge data from the SLOSH model is currently the best data publicly available for our purposes, and efforts have been made to ensure the validity of the SLOSH data in performing comparisons with tsunami inundation.

The SLOSH MOM results provide the worst-case storm surge for a given hurricane category and initial tide level based on a set of model runs with various combinations of parameters such as forward speed, trajectory, and landfall location. To perform the storm surge and tsunami comparisons, SLOSH storm surge elevation data was first converted to meters and adjusted from the NAVD88 to the MHW vertical datum using NOAA's VDatum tool (http://vdatum.noaa.gov/). Due to the relatively low resolution of the SLOSH data as compared to the DEMs used for tsunami modeling, the SLOSH data was interpolated to 1/3 arcsecond (10 m) resolution using a kriging method. Inundation was then determined by subtracting land elevation from the storm surge elevation.

Here, an initial high tide level is used for the SLOSH MOM results in order to compare the worst-case tsunami inundation with a worst-case storm surge scenario. The high tide SLOSH MOM data includes effects of the highest predicted tide level at each location. In comparison, water elevations in the tsunami modeling are based on the MHW datum, which averages the high water levels over the National Tidal Datum Epoch (NTDE). Within the

GOM, tidal ranges are relatively small, with diurnal ranges on the order of 1.5 ft (0.5 m) for most of the communities studied here, and slightly higher at around 2.5 ft (0.8 m) for the west coast of Florida. Thus, differences between highest tide levels and the mean of the highest tide levels are expected to be relatively small, though local bathymetric effects combined with tidal effects can still be significant.

It should be noted that the updated Saffir-Simpson Hurricane Wind Scale which delineates hurricane categories 1-5 does not include storm surge as a component of the measure of hurricane intensity and that other methods may capture the physics of hurricane severity and damage in a more appropriate manner (e.g. Kantha [2006], Basco and Klentzman [2006], Irish and Resio [2010]). However, the SLOSH MOM results take into account thousands of scenarios for a given hurricane category, resulting in a composite worst-case storm surge scenario for each Saffir-Simpson hurricane category. Thus, since hurricane preparedness, storm surge evacuation zones, and hazard mitigation efforts are based on hurricane category assignment, we aim to determine the hurricane category which produces MOM storm surge inundation ζ_h that is a best match to the tsunami MOM inundation ζ_t. That is, we determine the hurricane category which satisfies

$$min_c(|\zeta_{h_c} - \zeta_t|), \qquad c = \text{Cat1,..,Cat5} \tag{1}$$

for each grid cell. The inundation level for the best-match category is denoted $\zeta_{h_{min}}$. The actual difference between hurricane and tsunami inundation levels $\Delta\zeta = \zeta_{h_{min}} - \zeta_t$ then indicates how close of a match the best-match category actually is. Thus, positive values of $\Delta\zeta$ indicate where hurricane storm surge inundation is higher than tsunami inundation, and negative values indicate where tsunami inundation is higher. A common local practice in tsunami modeling is to only consider inundation above a threshold of 0.3 m (1 ft) [Horrillo et al., 2011, 2015]. This is due to the extensive flat and low-lying elevation found along the Gulf Coast. All depths are calculated for tsunami inundation modeling, but inundation less than 0.3 m (1 ft) is considered negligible here for inundation mapping purposes. Thus, comparisons are only made where either the tsunami or hurricane MOM inundation is at least 0.3 m (1 ft). Results for the one selected Gulf Coast community are given in the following subsections. It is possible that tsunami inundation zone has no hurricane flooding, therefore matching with hurricane category cannot be made.

5.1 Mississippi

Gulfport, MS (grid 4)

Fig. 38 shows the MOM tsunami inundation affecting areas from Waveland, Bay St. Louis, Pass Christian, Long Beach, and Gulfport. Overall the inundation is very low (¡ 0.2 m), scattered around the St Louis Bay and Big Lake. Unlike most other mapping areas, where the Mississippi Canyon landslide is responsible for the MOM inundation, here it is Probabilistic Submarine Landslide C (see Fig. 40).

The hurricane category which best matches the tsunami inundation in Gulfport, MS mapping area is shown in Fig. 42, and Fig. 43 shows $\Delta\zeta$ for the best-matching hurricane category satisfying Eq. 1. The hurricane category that best matches tsunami inundation is

Category 1, and the difference between hurricane flooding and tsunami inundation is ¿ 1 m, indicating that tsunami inundation is much lower than that of the Category 1 storms.

Pascagoula, MS (grid 5)

Fig. 39 shows the MOM tsunami inundation affecting Pascagoula, MS. Overall water depth exhibits decreasing trend from oceanfront toward the inland and from east to west, with maximum over 1.2 m. The east-to-west diminishing trend is due to the west portion being shielded from direct tsunami waves coming from the GOM through the barrier islands. Most of the inundated areas west of Pascagoula are unpopulated, like the Deer Island, the Bellefontaine Marsh and the Pascagoula River Marsh Coastal Preserve. In Pascagoula, there are very few populated places affected by the inundation, like south of the Beach Blvd and around the Greenwood Island. The Mississippi Canyon landslide is responsible for the MOM inundation (see Fig. 41).

The hurricane category which best matches the tsunami inundation in Pascagoula, MS mapping area (grid 5) is shown in Fig. 44, and Fig. 45 shows $\Delta\zeta$ for the best-matching hurricane category satisfying Eq. 1. The hurricane category that best matches tsunami inundation is also Category 1. The difference between hurricane flooding and tsunami inundation is mostly within 1 m for the eastern part and over 1 m for the rest Category 1 areas.

Mississippi
All Sources
SLOSH Storm Surge and MOM Tsunami Inundation Comparison

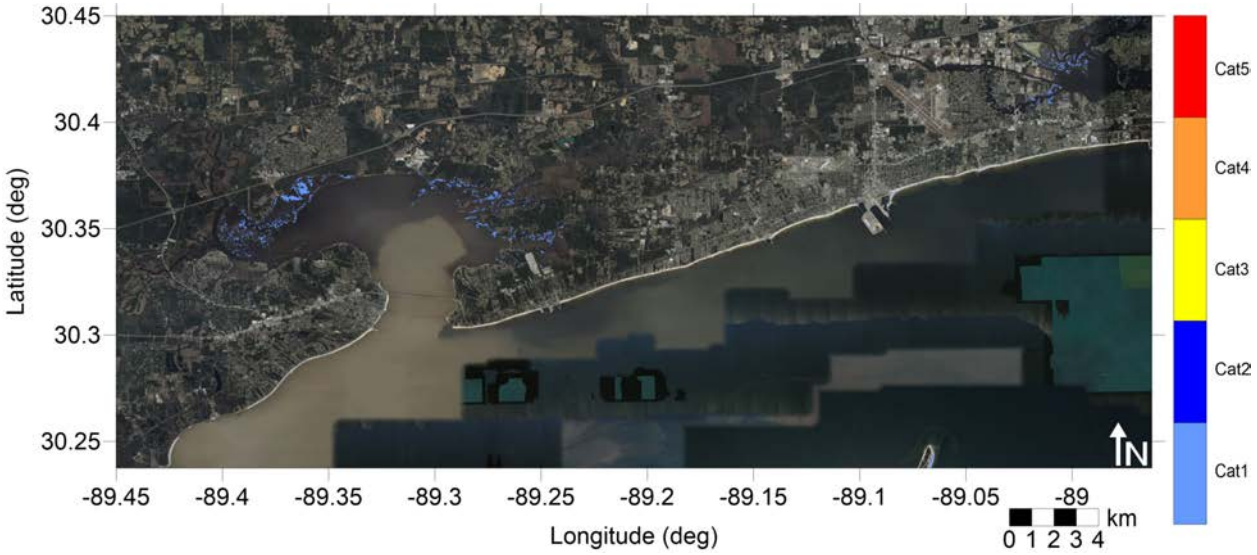

Figure 42: Hurricane category which produces inundation at high tide that best matches the MOM tsunami inundation shown in Figure **??** for Gulfport, MS. The contours drawn and labeled are at -5 m, -10 m, and -15 m levels.

Mississippi
All Sources
SLOSH Storm Surge and MOM Tsunami Inundation Comparison

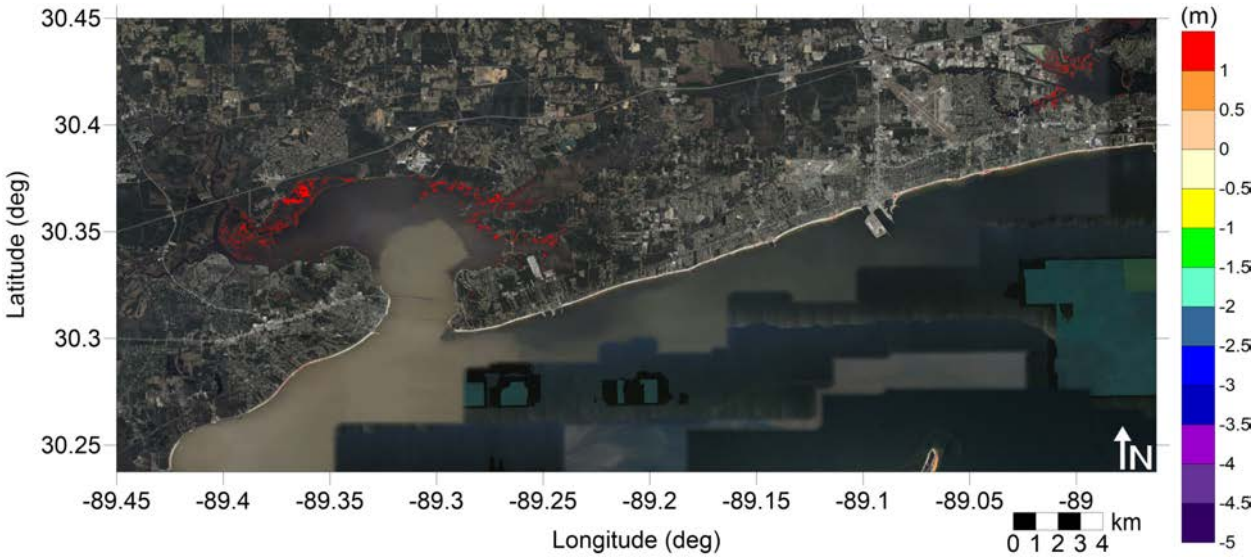

Figure 43: Actual difference $\Delta\zeta$ (in meters) between SLOSH MOM storm surge inundation and MOM tsunami inundation for the best-match hurricane category shown in Figure **??** for Gulfport, MS. Note that negative values indicate where tsunami inundation is higher than hurricane inundation, and pale colors indicate relatively good agreement between tsunami and storm surge inundation, i.e. $|\Delta\zeta| \leq 0.5$ m. The contours drawn and labeled are at -5 m, -10 m, and -15 m levels.

Mississippi
All Sources
SLOSH Storm Surge and MOM Tsunami Inundation Comparison

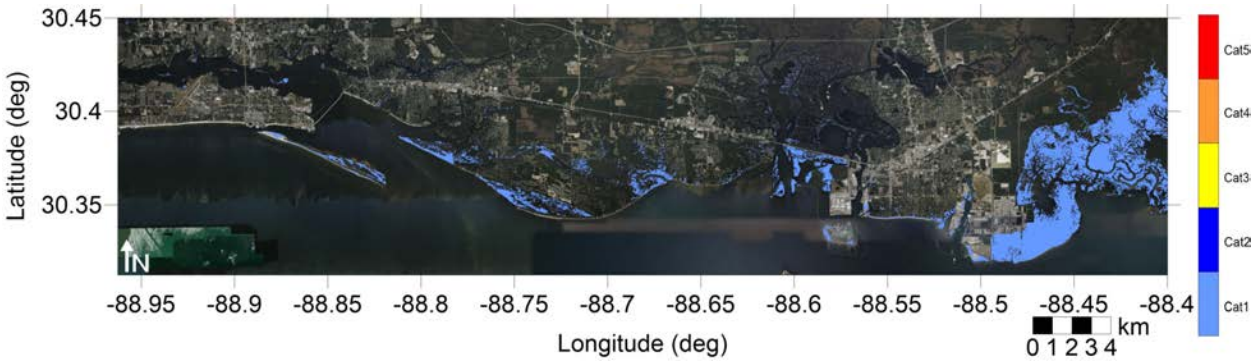

Figure 44: Hurricane category which produces inundation at high tide that best matches the MOM tsunami inundation shown in Figure **??** for Pascagoula, MS. The contours drawn and labeled are at -5 m, -10 m, and -15 m levels.

Mississippi
All Sources
SLOSH Storm Surge and MOM Tsunami Inundation Comparison

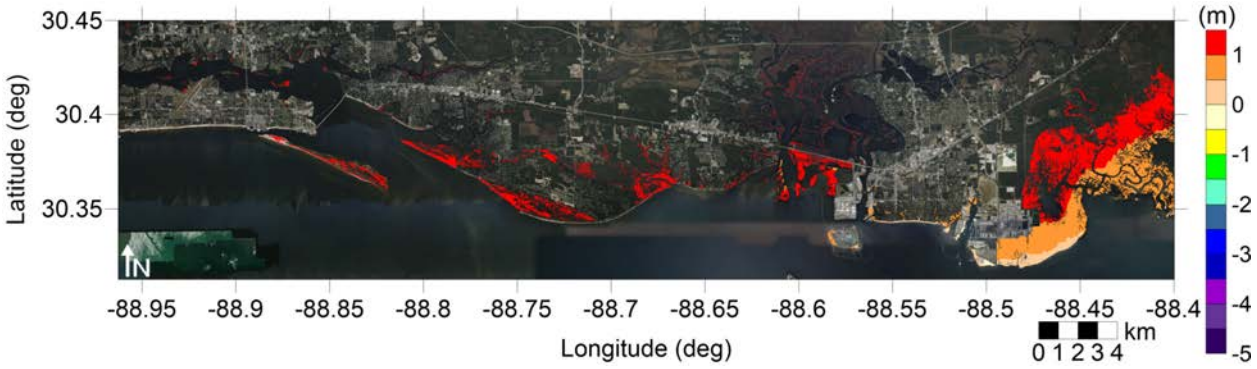

Figure 45: Actual difference $\Delta\zeta$ (in meters) between SLOSH MOM storm surge inundation and MOM tsunami inundation for the best-match hurricane category shown in Figure **??** for Pascagoula, MS. Note that negative values indicate where tsunami inundation is higher than hurricane inundation, and pale colors indicate relatively good agreement between tsunami and storm surge inundation, i.e. $|\Delta\zeta| \leq 0.5$ m. The contours drawn and labeled are at -5 m, -10 m, and -15 m levels.

6 Tsunami Maritime Products

Accurate estimates of tsunami wave amplitude do not necessarily equate to the prediction of localized damaging currents in a basin or harbor [Lynett et al., 2012]. Furthermore, damage potential in ports is strongly related to the current speed. Therefore, tsunami hazard mitigation products need to be advanced to predict damage potential in basins or harbors. Past tsunamis have shown that the maritime community requires additional information and guidance about tsunami hazards and post-tsunami recovery [Wilson et al., 2012, 2013]. To accomplish mapping and modeling activities to meet NTHMP's planning/response purposes for the maritime community and port emergency management and other customer requirements, it is necessary to continue the process to include maritime products in our current inundation map development. These maritime products will help identify impact specifically on ship channels, bay inlets, harbors, marinas, and oil infrastructures (e.g., designated lightering and oil tanker waiting zones).

In this study, the Mississippi coastal communies – Gulfport (grid 4) and Pascagoula (grid 5) – are added to the maritime portfolio, where tsunami hazard maritime products such as tsunami current magnitude, vorticity, safe/hazard zones are generated.

Lynett et al. [2014] complied a general relationship between tsunami current speed and harbor damage based on observational data, in which the current speed is divided into four ranges of damaging potential, 0 - 3 knots means unharmful currents, 3 - 6 knots corresponds to minor-to-moderate damage, 6 - 9 knots moderate-to-major damage, and over 9 knots extreme damage. Since the extent of damage is very location-dependent, to make the text concise, we associate 0 - 3 knots to unharmful currents, 3 - 6 knots to minor damage, 6 - 9 knots to moderate damage, and finally over 9 knots to major damage. The four levels are denoted with white, blue, yellow and red colors, respectively, for all the velocity contour plots within our velocity maritime products.

Using this damage-to-speed relationship, we have plotted the maximum of maximum depth-averaged velocity for each computational subdomain of the two new communities. Fig. 46 shows the minimum offshore safe depth (approximately 200 m or 100 fathoms), and the maximum of maximum velocity magnitude contour plot across the entire Gulf of Mexico (15 arcsecond resolution) for all landslide scenarios (Eastbreaks, PSL-A, PSL-B1, PSL-B2, Mississippi Canyon, PSL-C, West Florida, Yucatán #3 and Yucatán #5). Potential damaging currents ($>$ 3 knots, blue, yellow and red areas) tend to be present in most of the area shallower than the minimum offshore safe depth. However, damaging currents could reach areas deeper than 200 m close to most of the landslide generation regions. Major damaging currents ($>$ 9 knots, red) can be expected in most of the landslide generation regions, in the continental shelf adjacent to Mississippi Canyon, offshore northwest Florida, and Yucatán shelf. Moderate ($>$ 6 knots and $<$ 9 knots, yellow) damaging current areas are scattered over the continental shelf, but mostly close to areas with major damage currents.

All locations
All Sources
Maximum of Maximum Velocity Magnitude

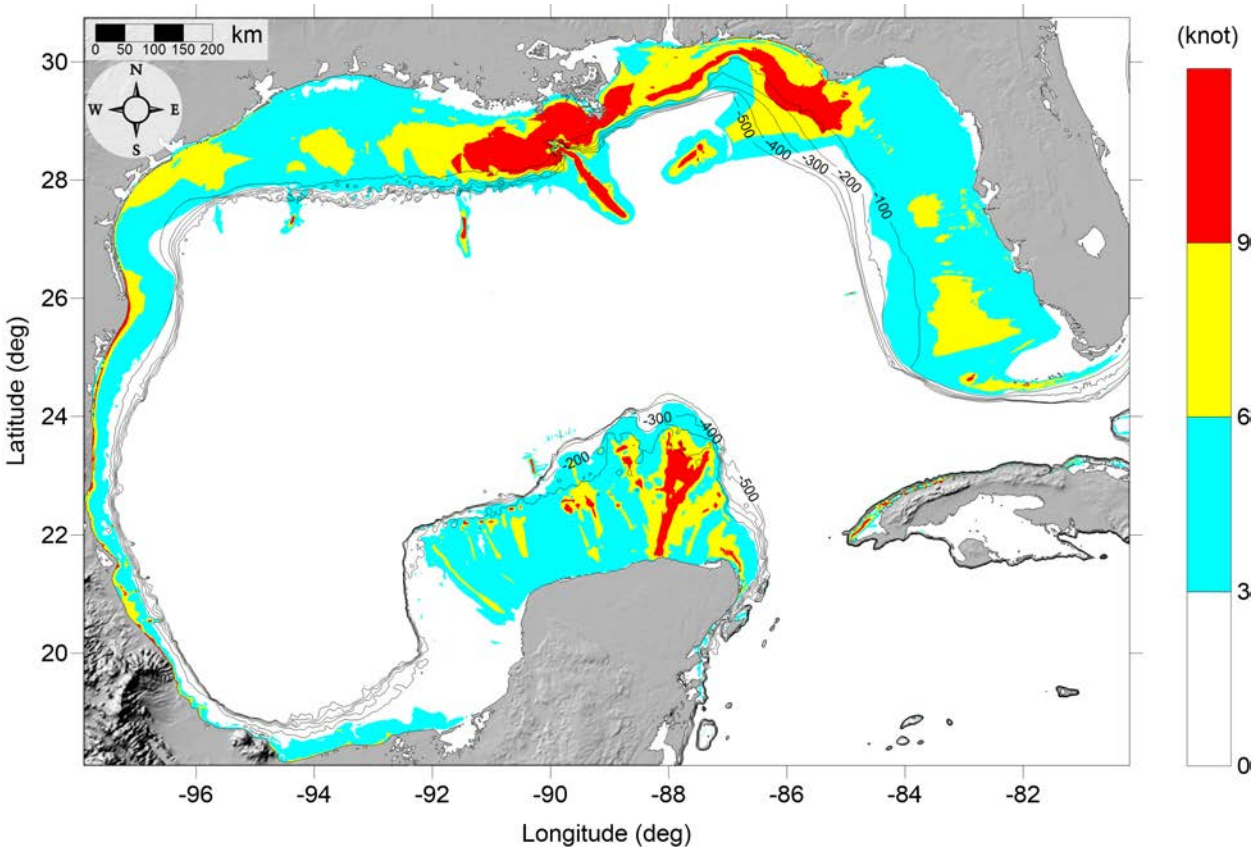

Figure 46: Maximum of maximum velocity magnitude contour in Mississippi (Grid 1 - 15 arcsecond) for all landslide scenarios.

The MOM velocity magnitude (damaging potential) contour maps and the MOM vorticity magnitude contour maps for the finer computational subdomains of Mississippi are presented from Fig. 47 to Fig. 53. Fig. 49 and Fig. 50 shows the MOM velocity magnitude contour plot result for the Gulfport and Pascagoula areas, respectively. Most of offshore region is expected to have no damaging currents, except the minor damaging currents occurring along the eastmost region of the Pascagoula grid. For both Gulfport and Pascagoula, vorticity distribution displays similar patterns to their velocity distribution, where highest vorticity appears around the east, although being very small (compared to other mapping areas).

6.1 Gulfport, MS

Mississippi
All Sources
Maximum of Maximum Velocity Magnitude

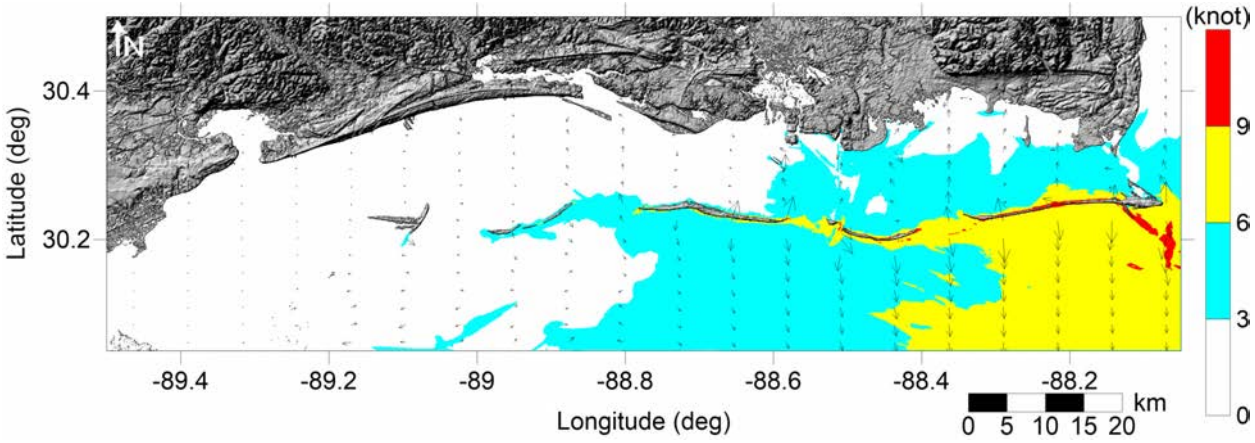

Figure 47: Maximum of maximum velocity magnitude contour in Mississippi (Grid 2 - 3 arcsecond) for all landslide scenarios.

Mississippi
All Sources
Maximum of Maximum Velocity Magnitude

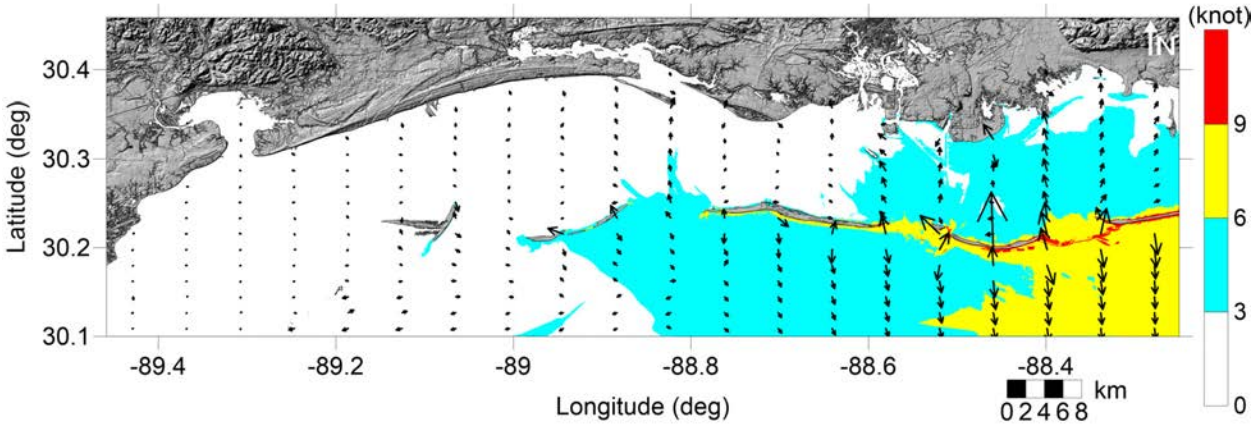

Figure 48: Maximum of maximum velocity magnitude contour in Mississippi (Grid 3 - 1 arcsecond) for all landslide scenarios.

Mississippi
All Sources
Maximum of Maximum Velocity Magnitude

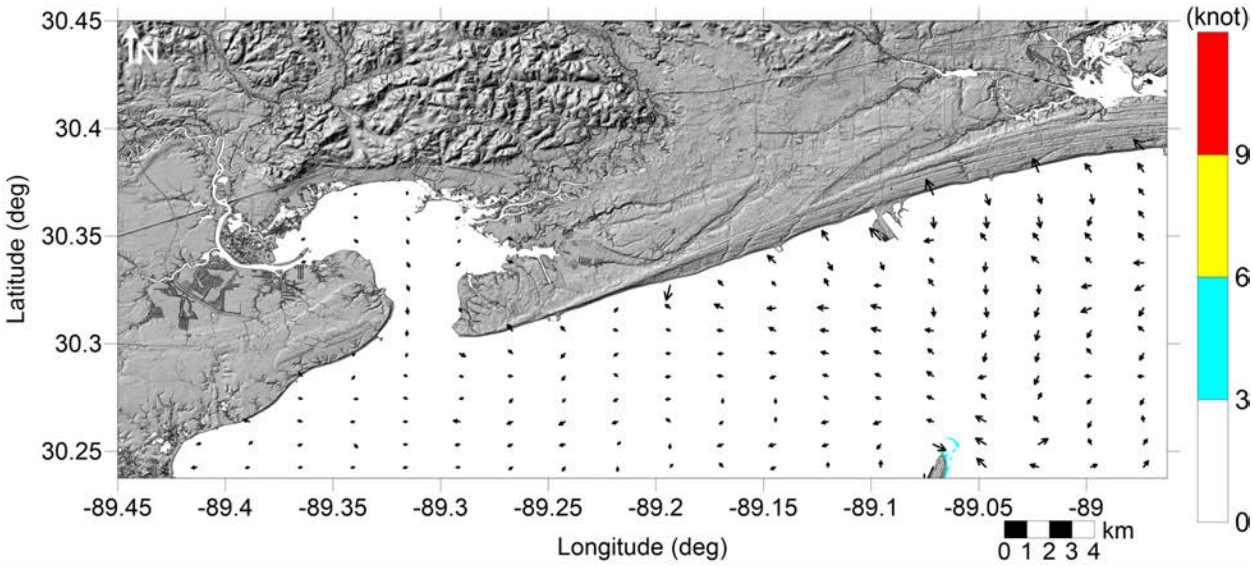

Figure 49: Maximum of maximum velocity magnitude contour in Gulfport, MS (Grid 4 - 1/3 arcsecond) for all landslide scenarios.

Mississippi
All Sources
Maximum of Maximum Velocity Magnitude

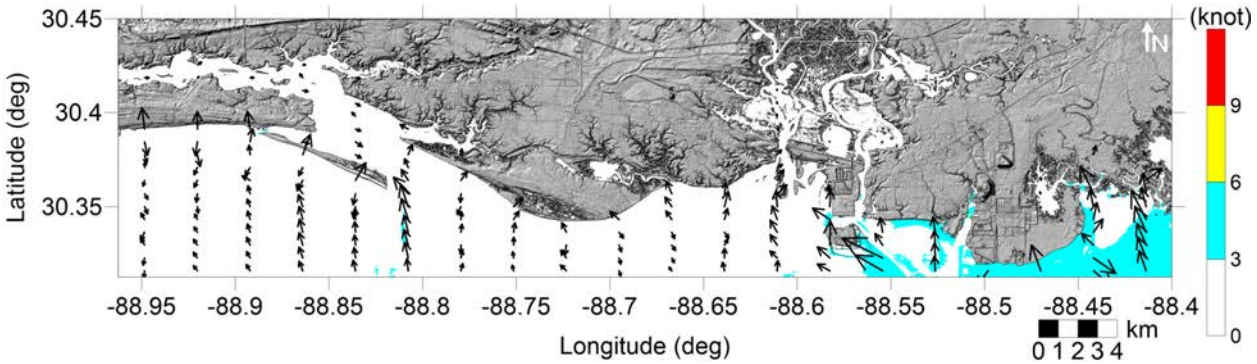

Figure 50: Maximum of maximum velocity magnitude contour in Pascagoula, MS (Grid 5 - 1/3 arcsecond) for all landslide scenarios.

Mississippi
All Sources
Maximum of Maximum Vorticity Magnitude

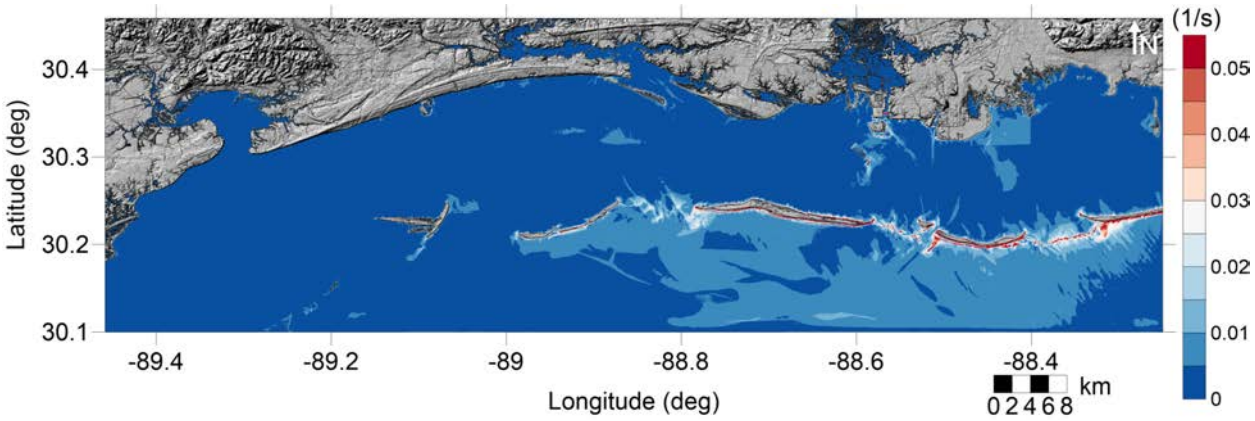

Figure 51: Maximum of maximum vorticity magnitude contour in Mississippi Grid 3 (1 arcsecond) for all landslide scenarios.

Mississippi
All Sources
Maximum of Maximum Vorticity Magnitude

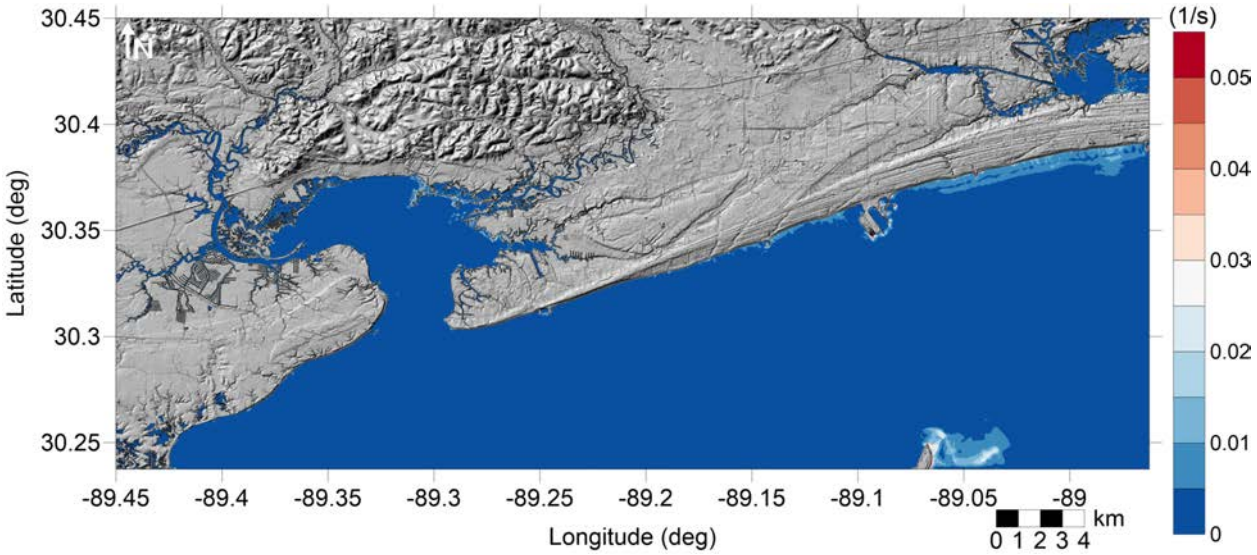

Figure 52: Maximum of maximum vorticity magnitude contour in Gulfport, MS Grid 4 (1/3 arcsecond) for all landslide scenarios.

Mississippi
All Sources
Maximum of Maximum Vorticity Magnitude

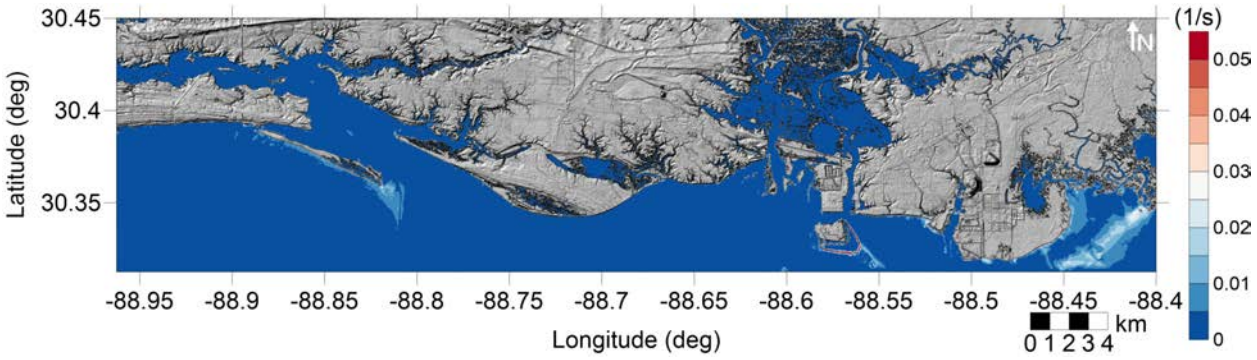

Figure 53: Maximum of maximum vorticity magnitude contour in Pascagoula, MS Grid 5 (1/3 arcsecond) for all landslide scenarios.

7 Conclusions

This project focused on the implementation of recent developments in the tsunami science recommended by the National Tsunami Hazard Mitigation Program - Modeling Mapping Subcommittee - Strategic Plan (NTHMP-MMS-SP) into our current Gulf of Mexico (GOM) tsunami mitigation products. Three main developments for tsunami mitigation have been created under this project for one new community in the GOM (Mississippi) that will provide guidance to state emergency managers for tsunami hazard mitigation and warning purposes. The first task is the development of tsunami inundation maps for the one selected community with nine landslide sources. The second is the comparison between existing SLOSH hurricane flooding data and our tsunami inundation result for the two new communities in order to facilitate temporal-low-order estimate for tsunami hazard areas (community) where inundation studies have not yet been assigned/executed or where little bathymetric and elevation data exists. The third is to produce maritime products (maximum of maximum (MOM) velocity and velocity magnitude maritime maps) for both communities to help identify impact specifically on ship channels, bay inlets, harbors, marinas, and other infrastructures.

Tsunami wave propagation and inundation in Mississippi was modeled to obtain maximum inundation and extent, momentum flux, current velocity and vorticity maps considering the entire suite of nine landslide sources.

In Gulfport area (grid 4, including Waveland, Bay St. Louis, Pass Christian, Long Beach, and Gulfport), overall the inundation is very low (¡ 0.2 m), scattered around the St Louis Bay and Big Lake. Unlike most other mapping areas, where the Mississippi Canyon landslide is responsible for the MOM inundation, here it is Probabilistic Submarine Landslide C (see Fig. 40).

In Pascagoula area (grid 5), the overall water depth exhibits decreasing trend from oceanfront toward the inland and from east to west, with maximum over 1.2 m. The east-to-west diminishing trend is due to the west portion being shielded from direct tsunami waves coming from the GOM through the barrier islands. Most of the inundated areas west of Pascagoula are unpopulated, like the Deer Island, the Bellefontaine Marsh and the Pascagoula River Marsh Coastal Preserve. In Pascagoula, there are very few populated places affected by the inundation, like south of the Beach Blvd and around the Greenwood Island. The Mississippi Canyon landslide is responsible for the MOM inundation (see Fig. 41).

While high-resolution tsunami inundation studies have been completed for these 20 communities and are planned for additional locations, vulnerability assessments are still essential for coastal locations where inundation studies have not yet been performed or planned, or where there is a lack of high-resolution bathymetric and/or elevation data. Therefore, we aim to extend the results of the completed mapping studies in order to provide estimates of tsunami inundation zones for hazard mitigation efforts in unmapped locations. We anticipate that communities which lack detailed tsunami inundation maps, but which have modeled hurricane storm surge information, would be able to use the results presented here to estimate their potential tsunami hazard level based on their regional topographical/bathymetric features. We stress, however, that such results should be used only in a broad, regional sense given the differences seen among and within communities based on local details of bathymetry, topography, and geographical location within the GOM basin. There is no

guarantee that comparison results will be identical in areas with similar topography, and comparisons should only be made after understanding the limitations and simplifications of the methodology presented here. Comparisons of MOM tsunami inundation results with the SLOSH MOM high tide storm surge inundation indicate that while the details of referencing tsunami inundation to hurricane storm surge is dependent on local topographic effects, general regional trends can be identified.

In Gulfport area (grid 4, including Waveland, Bay St. Louis, Pass Christian, Long Beach, and Gulfport), the hurricane category which best matches the tsunami inundation in Gulfport, MS mapping area is shown in Fig. 42, and Fig. 43 shows $\Delta\zeta$ for the best-matching hurricane category satisfying Eq. 1. The hurricane category that best matches tsunami inundation is Category 1, and the difference between hurricane flooding and tsunami inundation is $>$ 1 m, indicating that tsunami inundation is much lower than that of the Category 1 storms.

In Pascagoula area (grid 5), the hurricane category which best matches the tsunami inundation in Pascagoula, MS mapping area (grid 5) is shown in Fig. 44, and Fig. 45 shows $\Delta\zeta$ for the best-matching hurricane category satisfying Eq. 1. The hurricane category that best matches tsunami inundation is also Category 1. The difference between hurricane flooding and tsunami inundation is mostly within 1 m for the eastern part and over 1 m for the rest Category 1 areas.

We produced the MOM velocity and vorticity magnitude maps for all the landslide scenarios, for Orange Beach, AL and Mexico Beach, FL, based on a simplified current velocity damage scale where we associate 0 - 3 knots to unharmful currents, 3 - 6 knots to minor damage, 6 - 9 knots to moderate damage, and over 9 knots to major damage. The four damage levels are denoted with white, blue, yellow and red colors, respectively.

From the MOM velocity magnitude results in the entire Gulf of Mexico, it can be observed that, potential damaging currents ($>$ 3 knots, blue, yellow and red areas) tend to be present in most of the area shallower than the minimum offshore safe depth (approximately 200 m or 100 fathoms). However, damaging currents could reach areas deeper than 200 m close to most of the landslide generation regions. Major damaging currents ($>$ 9 knots, red) can be expected in most of the landslide generation regions, in the continental shelf adjacent to Mississippi Canyon, offshore northwest Florida, and Yucatán shelf. Moderate ($>$ 6 knots and $<$ 9 knots, yellow) damaging current areas are scattered over the continental shelf, but mostly close to areas with major damage currents.

For the Mississippi coastlines, most of offshore region is expected to have no damaging currents, except the minor damaging currents occurring along the eastmost region of the Pascagoula grid. For both Gulfport and Pascagoula, vorticity distribution displays similar patterns to their velocity distribution, where highest vorticity appears around the east, although being very small (compared to other mapping areas).

Tsunami hazard maritime products such as tsunami current magnitude, vorticity, safe/hazard zones would be central for future developments of maritime hazard maps, maritime emergency response and as well as infrastructure planning.

Although the recurrence of destructive tsunami events have been verified to be quite low in the GOM, our work has confirmed that submarine landslide events with similar characteristics to those used here, have indeed the potential to cause severe damage to GOM

coastal communities. Therefore, this work is intended to provide guidance to local emergency managers to help managing urban growth, evacuation planning, and public education with the final objective to mitigate potential landslide tsunami in the GOM.

Acknowledgments

This work was supported by the National Oceanic and Atmospheric Administration (NOAA) under awards NA23NWS4670020, "Tsunami Inundation Maps Development for the Gulf of Mexico". The authors wish to thank all NTHMP modeling and Mapping Subcommittee members and GOM's emergency manager representatives for their helpful insights. High resolution inundation maps are available from `http://www.tamug.edu/tsunami/NTHMP/NTHMP.html` or by contacting corresponding author.

References

D. Basco and C. Klentzman. On the classification of coastal storms using principles of momentum conservation. In *Proc. 31st Int. Conf. on Coastal Eng.* ASCE, 2006.

J. D. Chaytor, E. L. Geist, C. K. Paull, D. W. Caress, R. Gwiazda, J. U. Fucugauchi, and M. R. Vieyra. Source characterization and tsunami modeling of submarine landslides along the yucatán shelf/campeche escarpment, southern gulf of mexico. *Pure and Applied Geophysics*, 173(12):4101–4116, Dec 2016. ISSN 1420-9136. doi: 10.1007/s00024-016-1363-3. URL `https://doi.org/10.1007/s00024-016-1363-3`.

W. Cheng, J. Horrillo, and R. Sunny. Numerical analysis of meteotsunamis in the northeastern gulf of mexico. *Natural Hazards*, Sep 2021. ISSN 1573-0840. doi: 10.1007/s11069-021-05009-9.

B. Dugan and J. Stigall. Origin of overpressure and slope failure in the Ursa region, northern Gulf of Mexico. In D. C. Mosher, R. C. Shipp, L. Moscardelli, J. D. Chaytor, C. D. P. Baxter, H. J. Lee, and R. Urgeles, editors, *Submarine Mass Movements and Their Consequences*, pages 167–178. Springer Netherlands, 2010.

P. K. Dunbar and C. S. Weaver. *U.S. States and Territories National Tsunami Hazard Assessment: Historical Record and Sources for Waves*. U.S. Department of Commerce, National Oceanic and Atmospheric Administration, National Geophysical Data Center Tech. Rep.No. 3, 2008.

E. L. Geist, J. D. Chaytor, T. Parsons, and U. ten Brink. Estimation of submarine mass failure probability from a sequence of deposits with age dates. *Geosphere*, 9(2):287–298, 2013.

S. T. Grilli, O.-D. S. Taylor, C. D. P. Baxter, and S. Maretzki. A probabilistic approach for determining submarine landslide tsunami hazard along the upper east coast of the United States. *Mar. Geol.*, 264:74–97, 2009.

C. B. Harbitz, F. Løvholt, and H. Bungum. Submarine landslide tsunamis: How extreme and how likely? *Nat. Hazards*, 72(3):1341–1374, 2014.

C. W. Hirt and B. D. Nichols. Volume of fluid method for the dynamics of free boundaries. *J. Comput. Phys.*, 39:201–225, 1981.

J. Horrillo. *Numerical Method for Tsunami calculations using Full Navier-Stokes equations and the Volume of Fluid method*. PhD thesis, University of Alaska Fairbanks, 2006.

J. Horrillo, A. Wood, C. Williams, A. Parambath, and G. Kim. Construction of tsunami inundation maps in the Gulf of Mexico. Technical report, Award Number: NA09NWS4670006 to the National Tsunami Hazard Mitigation Program (NTHMP), National Weather Service Program Office, NOAA, 2011. avail. from http://www.tamug.edu/tsunami/NTHMP.html.

J. Horrillo, A. Wood, G.-B. Kim, and A. Parambath. A simplified 3-D Navier-Stokes numerical model for landslide-tsunami: Application to the Gulf of Mexico. *J. Geophys. Res.-Oceans*, 118:6934–6950, 2013. doi:10.1002/2012JC008689.

J. Horrillo, A. Pampell-Manis, C. Sparagowski, L. Parambath, and Y. Shigihara. Construction of five tsunami inundation maps for the Gulf of Mexico. Technical report, Award Number: NA12NWS4670014 and NA13NWS4670018 to the National Tsunami Hazard Mitigation Program (NTHMP), National Weather Service Program Office, NOAA, 2015. avail. from http://www.tamug.edu/tsunami/NTHMP.html.

J. Horrillo, W. Cheng, A. Pampell-Manis, and J. Figlus. Implementing nthmp-mms strategic plan in tsunami hazard mitigation products for the Gulf of Mexico. Technical report, Award Number: NA14NWS4670049 to the National Tsunami Hazard Mitigation Program (NTHMP), National Weather Service Program Office, NOAA, 2016. avail. from http://www.tamug.edu/tsunami/NTHMP.html.

J. Horrillo, W. Cheng, and J. Figlus. Development of four additional tsunami inundation maps with revision of Port Aransas, TX and updating existing ones with maritime products. Technical report, Award Number: NA15NWS4670031 and NA16NWS4670039 to the National Tsunami Hazard Mitigation Program (NTHMP), National Weather Service Program Office, NOAA, 2017. avail. from http://www.tamug.edu/tsunami/NTHMP.html.

J. Horrillo, W. Cheng, and J. Figlus. Development of two tsunami inundation maps in the GOM and inclusion of the USGS' Yucatan landslide tsunami sources. Technical report, Award Number: NA17NWS4670015 to the National Tsunami Hazard Mitigation Program (NTHMP), National Weather Service Program Office, NOAA, 2018. avail. from http://www.tamug.edu/tsunami/NTHMP.html.

J. J. Horrillo, W. Cheng, R. Sunny, A. Jose, and Y. Shang. Development of two tsunami inundation maps and continuation of the meteotsunami characterization for the gom. Technical report, Award Number: NA19NWS4670015 to the National Tsunami Hazard Mitigation Program (NTHMP), National Weather Service Program Office, NOAA, 2020. avail. from http://www.tamug.edu/tsunami/NTHMP.html.

J. J. Horrillo, W. Cheng, A. Jose, and Y. Shang. Development of two tsunami inundation maps and continuation of the meteotsunami characterization for the gom. Technical report, Award Number: NA20NWS4670066 to the National Tsunami Hazard Mitigation Program (NTHMP), National Weather Service Program Office, NOAA, 2021. avail. from http://www.tamug.edu/tsunami/NTHMP.html.

J. L. Irish and D. T. Resio. A hydrodynamics-based surge scale for hurricanes. *Ocean Eng.*, 37:69–81, 2010.

L. Kantha. Time to replace the Saffir-Simpson hurricane scale? *Eos, Transactions American Geophysical Union*, 87(1):3–6, 2006.

W. Knight. Model predictions of Gulf and Southern Atlantic Coast tsunami impacts from a distribution of sources. *Sci. of Tsunami Hazards*, 24:304–312, 2006.

A. M. López-Venegas, J. Horrillo, A. Pampell-Manis, V. Huérfano, and A. Mercado. Advanced tsunami numerical simulations and energy considerations by use of 3D - 2D coupled models: The October 11, 1918, Mona Passage tsunami. *Pure Appl. Geophys.*, 172(6):1679–1698, 2015.

P. J. Lynett, J. C. Borrero, R. Weiss, S. Son, D. Greer, and W. Renteria. Observations and modeling of tsunami-induced currents in ports and harbors. *Earth and Planetary Science Letters*, 327:68–74, 2012.

P. J. Lynett, J. Borrero, S. Son, R. Wilson, and K. Miller. Assessment of the tsunami-induced current hazard. *Geophysical Research Letters*, 41(6):2048–2055, 2014.

S. Maretzki, S. Grilli, and C. D. P. Baxter. Probabilistic SMF tsunami hazard assessment for the upper east coast of the United States. In V. Lykousis, D. Sakellariou, and J. Locat, editors, *Submarine Mass Movements and Their Consequences*, pages 377–385. Springer Netherlands, 2007.

D. Masson, C. Habitz, R. Wynn, G. Pederson, and F. Lovholt. Submarine landslides: Processes, triggers and hazard protection. *Philos. Trans. R. Soc. A*, 364:2009–2039, 2006.

A. Pampell-Manis, J. Horrillo, Y. Shigihara, and L. Parambath. Probabilistic assessment of landslide tsunami hazard for the northern Gulf of Mexico. *J. Geophys. Res.-Oceans*, 2016. doi:10.1002/2015JC011261.

C. K. Paull, D. W. Caress, R. Gwiazda, J. Urrutia-Fucugauchi, M. Rebolledo-Vieyra, E. Lundsten, K. Anderson, and E. J. Sumner. Cretaceous–paleogene boundary exposed: Campeche escarpment, gulf of mexico. *Marine Geology*, 357:392–400, 2014.

U. S. ten Brink, H. J. Lee, E. L. Geist, and D. Twichell. Assessment of tsunami hazard to the U.S. East Coast using relationships between submarine landslides and earthquakes. *Mar. Geol.*, 264:65–73, 2009a.

U. S. ten Brink, D. Twichell, P. Lynett, E. Geist, J. Chaytor, H. Lee, B. Buczkowski, and C. Flores. Regional assessment of tsunami potential in the Gulf of Mexico. *U. S. Geol. Surv. Admin. Rep.*, 2009b.

R. Wilson, C. Davenport, and B. Jaffe. Sediment scour and deposition within harbors in california (usa), caused by the march 11, 2011 tohoku-oki tsunami. *Sedimentary Geology*, 282:228–240, 2012.

R. I. Wilson, A. R. Admire, J. C. Borrero, L. A. Dengler, M. R. Legg, P. Lynett, T. P. McCrink, K. M. Miller, A. Ritchie, K. Sterling, et al. Observations and impacts from the 2010 chilean and 2011 japanese tsunamis in california (usa). *Pure and Applied Geophysics*, 170(6-8):1127–1147, 2013.

Y. Yamazaki, Z. Kowalik, and K. F. Cheung. Depth-integrated, non-hydrostatic model for wave breaking and run-up. *Int. J. Numer. Meth. Fl.*, 61:473–497, 2008.